A Search for Pre-Main Sequence Eclipsing Binaries and Stellar Rotation Periods in the Lagoon Nebula

By

Calen B. Henderson

Senior Honors Thesis

Submitted to the Faculty of the

Department of Physics and Astronomy of Vanderbilt University

In partial fulfillment of the requirements for

Departmental Honors in Physics

May, 2009

Adviser:
Keivan G. Stassun

Honors Thesis Committee:
Andreas A. Berlind
Norman H. Tolk
David A. Weintraub

Abstract

Rotation Periods, Eclipsing Binary Stars, NGC 6530, Lagoon Nebula, Pre-Main Sequence Stars, Time-Series Photometry

We report time-series CCD I-band photometry for the pre-main-sequence cluster NGC 6530, located within the Lagoon Nebula. The data were obtained with the 4Kx4K imager on the SMARTS 1.0m telescope at CTIO on 36 nights over the summers of 2005 and 2006. In total we have light curves for ~50,000 stars in an area ~1 deg^2, with a sampling cadence of ~1 hour. Approximately 1,000 of these stars have been identified as bona fide members of the cluster with masses in the range 0.25-4.0 M_{sun}, assuming a distance of 1.25 kpc to the cluster. Our goals are to measure rotation periods for these stars and to identify eclipsing binary candidates. Here we present light curves of the 223 stars in our sample found by us to be periodically variable, and we present the distribution of the stellar rotation periods derived from these light curves. We also present 16 potential eclipsing binary star systems that, through follow-up work, will provide direct measurements of the masses and radii of the stars for testing of stellar evolutionary models. This work has been supported by the National Science Foundation under Career grant AST-0349075.

I. Introduction

Figure I.I: A photo of M8, the Lagoon Nebula
Photo by: Michael Sherick
Retrieved from: http://antwrp.gsfc.nasa.gov/apod/ap050803.html

The Lagoon Nebula, more commonly referred to as M8, has, until recently, remained a largely unexplored region of star-formation. Embedded within the Lagoon Nebula is NGC 6530, a very young open star cluster. This cluster contains some several thousand young stars we can exploit to test basic theories of star formation.

Damiani et al. (2004) recently conducted a large-scale study of the stellar population of NGC 6530. Using the *Chandra X-Ray Observatory*, they detected 884 X-Ray point sources and proposed that 90%-95% constitute cluster members. In 2005, Prisinzano et al. performed a complementary deep optical study of NGC 6530. They were able to obtain BVI photometry down to a magnitude limit of V ~ 23 using the Wide Field Imager camera at the MPG/ESO 2.2 m telescope. They matched their catalog with that of the X-Ray observations of Damiani et al., and found a total of 828 common stars. Even more recently, Damiani et al. (2006) have increased the number of low-mass pre-main sequence (PMS) cluster members to more than 1100 by studying IR-excess emissions, which are indicative of young stars still surrounded by protoplanetary disks.

These studies provide a catalog of several hundred stars that have been confirmed as young pre-main sequence cluster members. With the sample selection already completed, the stage is set for a comprehensive synoptic study of NGC 6530. For my senior honors thesis research, I have been working with Dr. Keivan Stassun of the Vanderbilt Astronomy Department to begin such an analysis. The aims of the project can be described as follows.

We have imaged the Lagoon Nebula and are looking for eclipsing binary star systems and periodic variations indicative of rotation periods. By analyzing the light curves of identified eclipsing binary star systems, we can directly measure the stars' masses, radii, temperatures, and luminosities, and thus test current stellar evolution theories that predict specific relationships between these physical properties as a function of age. These relationships are important, as they are the basis for determining the fundamental properties of stars. Our measurements of these properties will test the basic theories that are central to the determination of stellar ages and masses. We will also examine the distribution of stellar rotation periods. This is essential to understanding how the angular momenta of stars evolve with time, a problem that remains one of the longest outstanding questions in star formation research.

In Section II we describe the data, how they were collected, and the methods used to analyze them. In Section III we discuss the results of the light curve analysis. In Section IV we discuss the implications of the results specifically in the context of how they addressed the problems described above. Section V will revisit and summarize the main points of the paper.

II. Data and Methods

Our aim is to monitor the Lagoon Nebula in search of stellar rotation periods and eclipsing binary candidates. We build off of the results of Prisinzano et al. (2005) and use their catalog as the basis for our study.

II.I Observations

We imaged the Lagoon Nebula periodically over 36 nights during the summers of 2005 and 2006. All data were taken using the Y4K Cam on the SMARTS 1.0m telescope at the Cerro Tololo Inter-American Observatory (CTIO), near La Serena, Chile. The Y4K Cam has a field of view of 20' x 20' square, and we divided the field into four quadrants and a center sub-field, alternating imaging each one. This gives us a full field of view of 40' x 40' square. We assumed a cluster center of RA = $18^h04^m24.2^s$ and DEC = -24°21′06″ so that our observations were coincident with the center assumed by Damiani et al. (2004), RA = $18^h04^m24.38^s$ and DEC = -24°21′05.8″, which is the center of the cluster NGC 6530. The assumed centers for each of the five fields, including the center, are shown in Table II.I.I. Two different exposure times were used, long (720s integration time) and short (7s integration time), to allow for complete magnitude coverage of the field. This resulted in time-series CCD I-band photometric data for some 10^4 stars on over 1200 images. Table II.I.II shows how many exposures of each length were taken of each field for night during the observing runs. An "x" indicates that the conditions were cloudy enough so as to preclude any observing. As is shown, no center field exposures were taken during the 2005 data run.

Table II.I.I: Field Centers

Field	RA	DEC
1	18:05:01.6	-24:12:34
2	18:05:01.6	-24:29:34
3	18:03:46.9	-24:29:34
4	18:03:46.9	-24:12:34
Center	18:04:24.2	-24:21:05
Damiani	**18:04:24.4**	**-24:21:06**

Figure II.I.I: The SMARTS consortium 1.0m telescope at CTIO

Table II.I.II: Observational Data

		2005						2006				
		7/8	7/9	7/10	7/11	7/12	7/13	6/15	6/16	6/17	6/18	6/19
Field1	Short	5	7	9	7	5	5	4	5	5	5	5
	Long	6	7	8	7	6	4	4	5	5	5	5
Field 2	Short	6	8	8	7	4	4	4	4	5	5	5
	Long	6	7	8	7	4	5	4	4	5	5	5
Field 3	Short	6	9	8	7	5	4	4	5	5	5	5
	Long	6	7	8	7	4	4	4	5	5	5	5
Field 4	Short	6	7	8	7	4	5	4	5	6	5	4
	Long	6	7	8	7	4	4	4	5	5	5	4
Center Field	Short	0	0	0	0	0	0	5	9	9	10	7
	Long	0	0	0	0	0	0	5	9	9	9	7

		2006										
		6/20	6/21	6/22	6/23	6/24	6/25	6/26	6/27	6/28	6/29	6/30
Field1	Short	5	4	4	0	3	4	4	3	4	2	3
	Long	5	4	4	0	2	4	4	3	4	2	3
Field 2	Short	5	4	4	0	3	4	4	3	4	2	3
	Long	5	4	4	0	2	4	4	3	4	2	3
Field 3	Short	5	4	4	0	3	3	4	3	4	2	3
	Long	5	4	4	0	2	3	4	3	4	2	2
Field 4	Short	5	4	4	0	3	4	4	4	4	2	3
	Long	5	4	3	0	2	3	3	3	3	2	2
Center Field	Short	8	8	8	1	6	8	8	6	8	3	6
	Long	8	8	7	1	5	7	7	6	7	3	5

Table II.I.II: Observational Data (continued)

		2006										
		7/1	7/2	7/3	7/4	7/5	7/6	7/7	7/8	7/9	7/10	7/11
Field1	Short	4	4	3	3	2	x	x	0	x	1	x
	Long	4	4	3	3	2	x	x	0	x	0	x
Field 2	Short	4	4	3	3	2	x	x	0	x	1	x
	Long	4	4	3	3	2	x	x	0	x	0	x
Field 3	Short	4	3	3	3	1	x	x	0	x	1	x
	Long	3	3	3	3	1	x	x	0	x	0	x
Field 4	Short	4	3	3	3	1	x	x	0	x	1	x
	Long	3	3	3	3	1	x	x	0	x	0	x
Center Field	Short	7	7	5	5	3	x	x	1	x	3	x
	Long	6	7	5	4	3	x	x	1	x	1	x

		2006							
		7/12	7/13	7/14	7/15	7/16	7/17	7/18	7/19
Field1	Short	x	4	3	3	3	3	3	3
	Long	x	4	3	3	3	3	3	3
Field 2	Short	x	3	3	3	3	3	3	3
	Long	x	3	3	3	3	3	3	3
Field 3	Short	x	2	3	3	3	3	3	3
	Long	x	2	3	3	3	3	3	3
Field 4	Short	x	2	3	3	3	3	3	2
	Long	x	2	3	3	3	3	3	2
Center Field	Short	x	6	6	6	6	6	6	5
	Long	x	6	6	6	6	6	6	5

II.II Methods

II.II.I CCD Reductions

Raw CCD images need to be calibrated, and we perform the following steps to achieve this, each of which will be explained in further detail: trimming and overscan subtraction, bias subtraction, flat field division, illumination correction, and shutter correction. Software packages within Image Reduction and Analysis Facility (IRAF) were used for all of the reductions. To elucidate the specifics of each stage, we follow a raw image as it goes through the entire reduction process.

Before conducting any science on our images, we need to reduce and calibrate them. The first step in this process is what is known as trimming and overscan-subtraction. Each of our exposures was taken using a CCD that measures 4104 by 4104 pixels. An example of a raw long-exposure science frame (an exposure of the scientifically interesting object(s)) of field 2 from the night of June 16, 2006, filename y060616.0121.fits, is shown in Figure II.II.I.I. However, only a region measuring 4058 by 4064 pixels contains real exposed pixels. The remaining pixels are blank pixels that

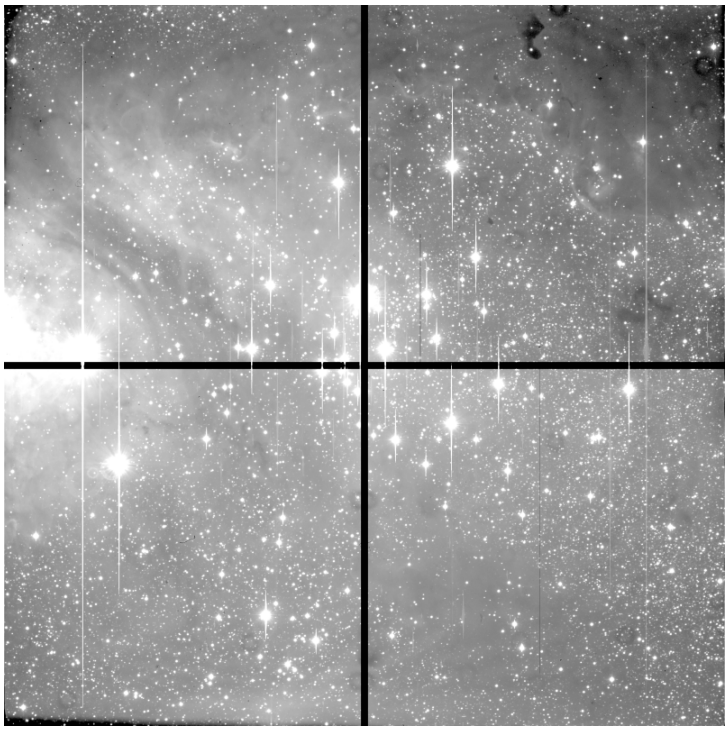

Figure II.II.I.I: A raw long-exposure science frame

form two strips that are centered horizontally and vertically and divide the image into four quadrants as shown. In addition there is a vertical region of virtual pixels, known as the overscan region, that is not exposed during observation. Before any observation, all pixels, including those in the overscan region, are given a set pedestal level of electrons,

creating a new zero-point, before readout takes place. This facilitates the measuring of all fluctuations in the background, not just the positive ones. The pixels in the overscan region are not exposed to light, so the value for these pixels represents only and approximately the exact pedestal amount, which must be subtracted off from all pixels as the first step of reduction. The IRAF routine CCDPROC will mean-average the values of all pixels in the overscan region and then subtract off this pedestal level from all pixels in the exposure. It will also trim off the blank strips of pixels. However, these two steps are done concurrently with the next step, bias-subtraction, so the first run through CCDPROC doesn't occur yet.

Though the overscan-subtraction removes the pedestal that is common to all pixels, it does not account for any pixel-to-pixel variations that might cause offsets in the zero-point. Correcting for that is accomplished via what are called bias or zero frames. Bias frames are taken while the shutter is closed and with a zero-second integration time, to ensure that the pixels receive no light. Using the ZEROCOMBINE routine within IRAF, these bias frames, usually 7-10 per night, are median-averaged and combined using a min/max rejection scheme that throws out the highest and lowest value for a given pixel across each image prior to the actual averaging. These two parameters in conjunction virtually guarantee that no cosmic rays contaminate the frames. The new frame, a master bias frame, will then be subtracted from each image. Now, rather than subtracting solely a single number from all pixels across all frames, a two-dimensional map of the pixel-to-pixel variations is subsequently subtracted from each image as well. The first run through CCDPROC will accomplish all of these tasks. It first subtracts the overscan pedestal, then trims the image, and finally subtracts the master bias frame from all images. It is important to note that the bias frames also underwent trimming and overscan-subtraction, so the zero-point for all images should average to zero. Figure II.II.I.II shows the master bias frame. Figure II.II.I.III shows the example science frame after it has undergone this first pass through CCDPROC.

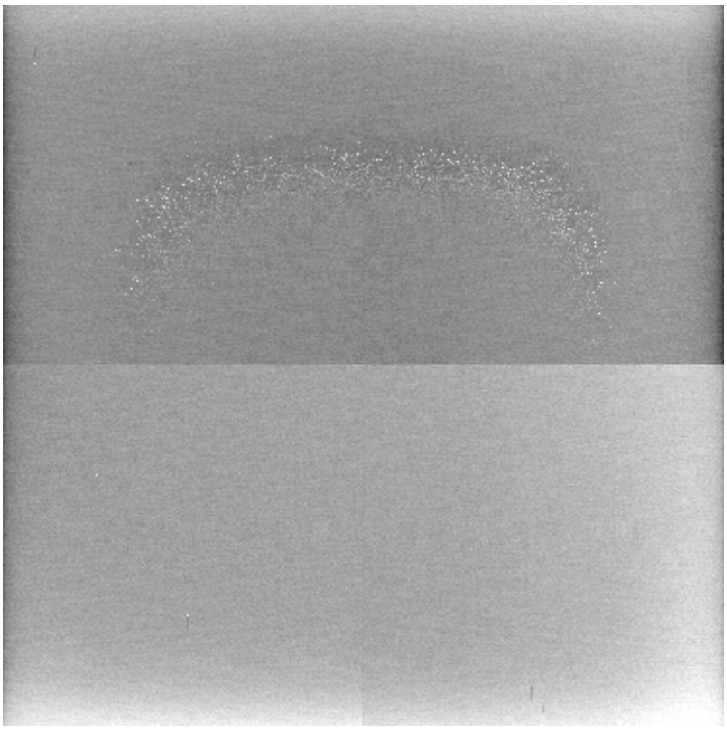

Figure II.II.I.II: The master bias frame

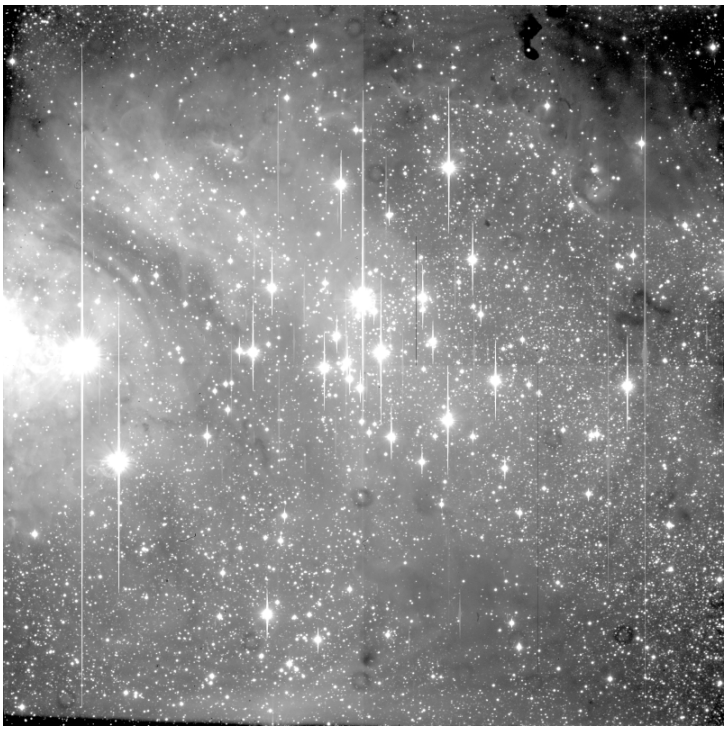

Figure II.II.I.III: The science frame after being trimmed, overscan-subtracted, and bias-subtracted

The next phase of image reduction corrects for varying pixel response functions. While all exposed pixels collect incident light, the throughput is not spatially constant for all pixels across the chip or temporally constant for a given pixel across time. Calibration frames called dome flats are used to normalize all of the pixel-response functions. Dome flats are typically taken during the afternoon preceding an observing night and are done with the dome of the observatory closed. Uniform brightness lamps illuminate a similarly uniformly white circle on the inside of the dome. Typically 7-10 dome flats are taken per filter (in our case, only the I-filter is necessary) per observing night. These frames are also trimmed, overscan-subtracted, and bias-subtracted. Using the IRAF routine FLATCOMBINE, all dome flats are then mean-averaged to create a master dome flat frame. Another pass through CCDPROC divides all object frames (sky flats and science frames) by this master dome flat, thus accounting for any variations in the pixel response functions. Figure II.II.I.IV shows the master dome flat frame. Figure II.II.I.V shows the science frame after its second pass through CCDPROC.

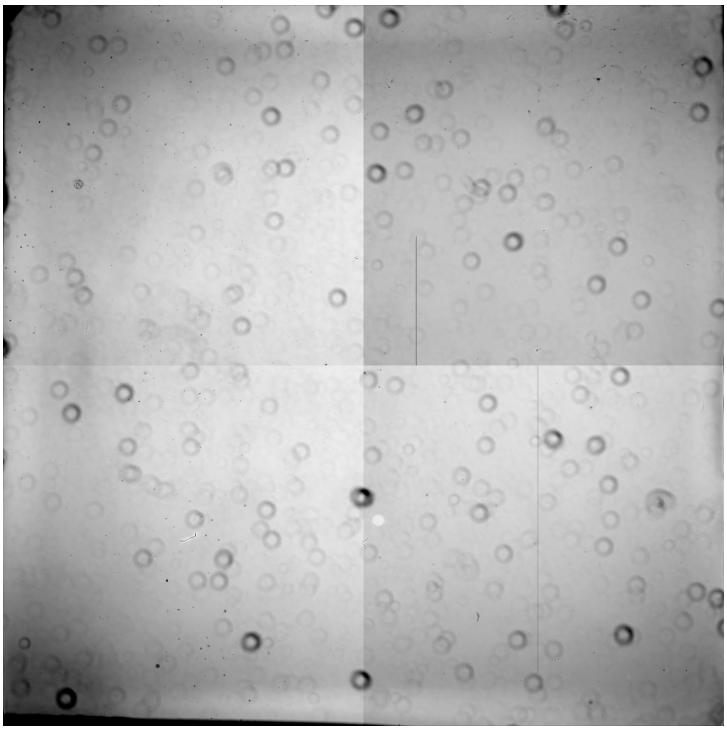

Figure II.II.I.IV: The master dome flat frame

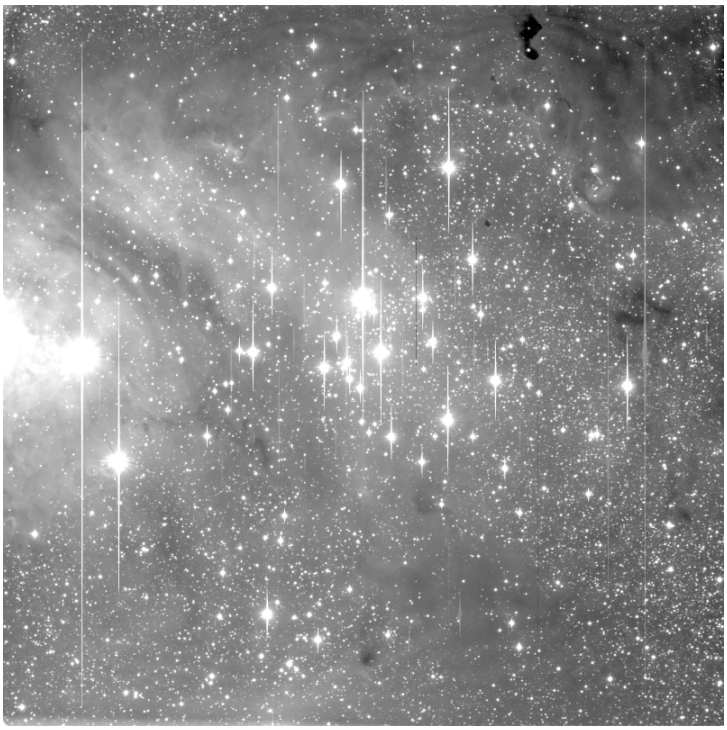

Figure II.II.I.V: The science frame after flat-field division

One final type of calibration frame must be used before all images are considered fully reduced. Termed sky flats, these are exposures that are taken of the twilight sky just prior to sunset. About three sky flats per filter are taken per night. Using the IRAF

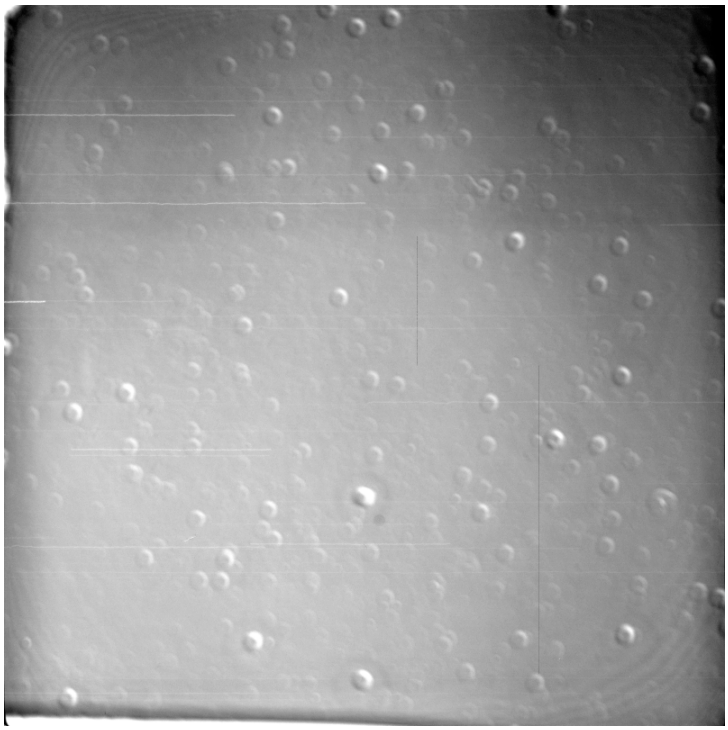

Figure II.II.I.VI: The master sky flat frame

Figure II.II.I.VII: The illumination correction frame

routine IMCOMBINE, these sky flats are mean-averaged and combined to produce a master sky flat frame. Next, the IRAF routine MKSKYCOR is used to smooth the master sky flat frame, creating an illumination correction frame. A third pass through CCDPROC divides all science frames by this illumination correction frame. Figures II.II.I.VI and II.II.I.VII show the master sky flat frame and the illumination correction frame, respectively. Figure II.II.I.VIII shows the science frame after the third and final pass through CCDPROC, when it is has been divided by the illumination correction frame. Now, half of the science frames are reduced and are ready to be processed.

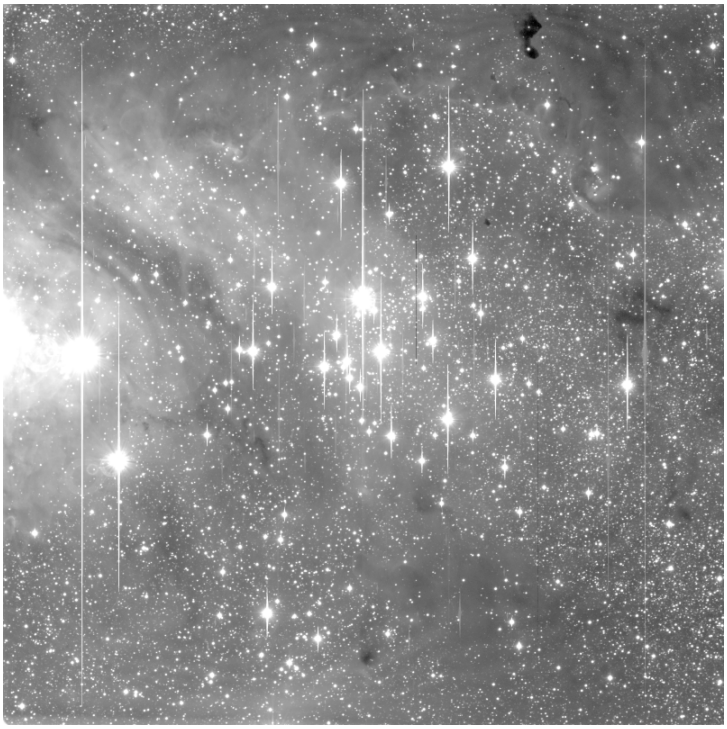

Figure II.II.I.VIII: The science frame after the illumination correction

The portion of the images not yet ready for processing is the short exposure frames, which have a 7-second integration time. The shutter on the Y4K Cam is a six-bladed iris that takes a finite time to open from the center out. Thus, the shutter exposes the center first and closes over the center last, creating a six-bladed iris pattern across the image. Exposures shorter than 10 seconds require a correction that is greater than 0.3 percent. Using the IRAF routine IMARITH, all short exposure frames are multiplied by this shutter correction image to reverse the effect of the non-uniform exposure time of the shutter. Figure II.II.I.IX shows the shutter correction frame. Figures II.II.I.X and II.II.I.XI show a short exposure image before and after the shutter correction is applied. Though perhaps not visually apparent, the correction is crucial to the performance of high-precision photometry on such short exposures. Once this stage is complete, all science frames have been effectively reduced and are ready to be processed.

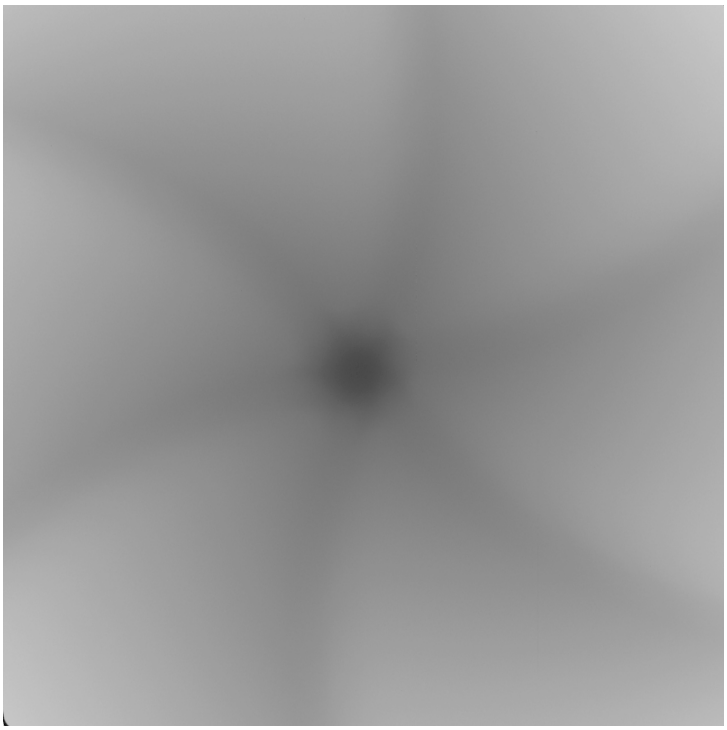

Figure II.II.I.IX: The shutter correction frame

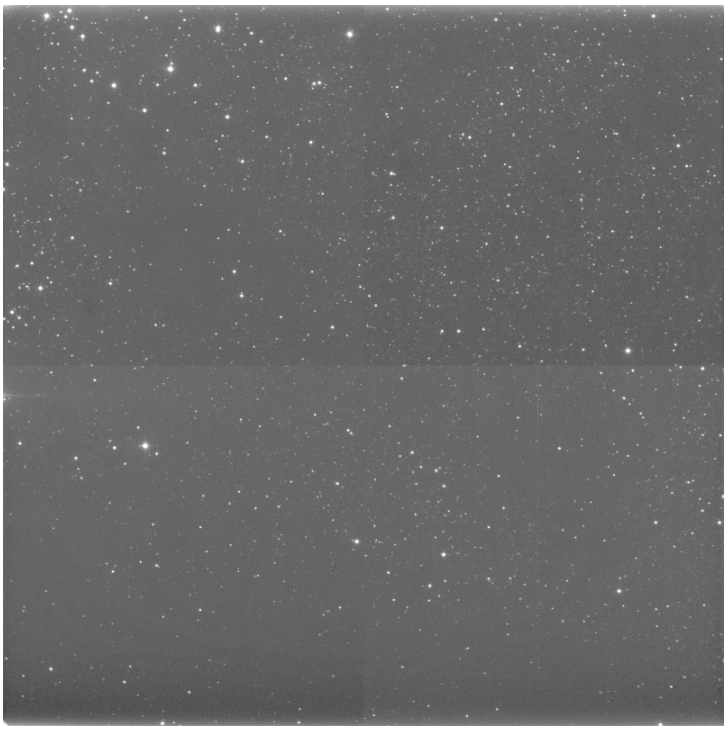

Figure II.II.I.X: A reduced short exposure frame prior to the shutter correction

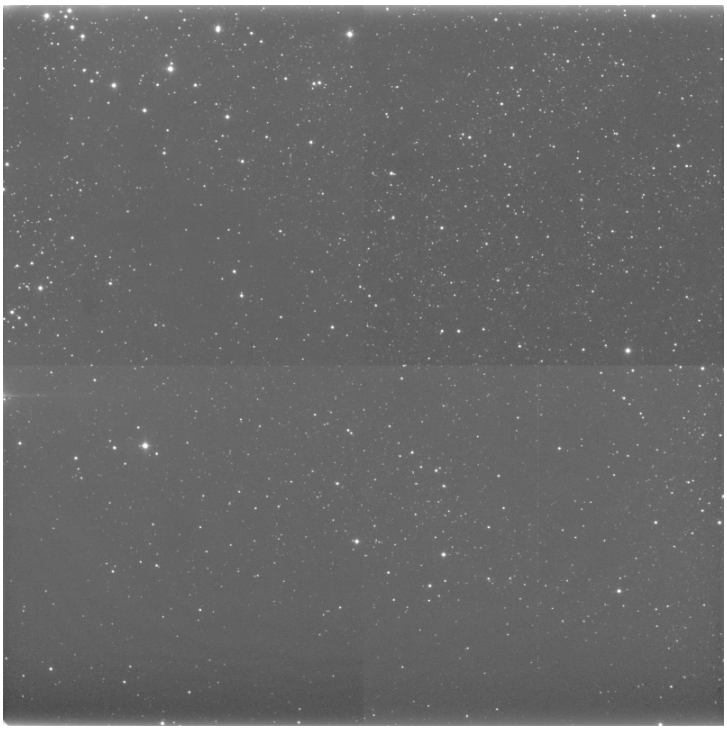

Figure II.II.I.XI: The short exposure frame after the shutter correction

II.II.II Image Processing

Once all science frames have been reduced, the next step is to find the stars of interest and extract their magnitudes. This was accomplished in the following stages, which will be explained in detail below: image registration, astrometric plate solution calculation, PSF photometry, extrinsic flux normalization, and final light curve production. In order to accomplish these steps, we run a custom software pipeline that utilizes both IRAF and IDL.

II.II.II.I Image Registration

Before the magnitude of each star can be measured, all science frames need to be registered to the same set of absolute coordinates. This guarantees that when a star is located on multiple frames it will be possible to discuss its position in absolute terms rather than relative (x,y) pixel coordinates. Since each of the five fields (1-4 and center) corresponds to a different region of the sky, this registration process is done ten different times: for the sets of long and short exposures of each field separately.

The first step is to pick an image with good seeing that will serve as a template reference image for that field. There must also be a different reference image whose absolute equatorial coordinates (Right Ascension and Declination) are known for the

field in question. For our purposes we use a Digital Sky Survey (DSS) image that corresponds to the region that contains NGC 6530.

After both reference images have been selected, the next step is to visually locate approximately twenty-five isolated and well-sampled stars that are common to both images. These stars will serve as reference stars for the entire field for the remainder of the registration process. The XYEQ package in IRAF computes absolute (equatorial) coordinates when given input pixel positions for an image whose header contains the frame's plate solution. By doing this for all 25 common reference stars, a table is generated with five columns: star ID (1-25, chosen arbitrarily), x coordinate, y coordinate, RA, and DEC. The x and y coordinate correspond to the pixel coordinates of the star on the non-DSS reference image while the RA and DEC are those extracted from the DSS image header by having IRAF look in the header and use the plate solution to apply the transformation. The absolute coordinates of the stars do not change by any significant amount between our reference image and the DSS reference image. Thus, the RA and DEC for these reference stars as they are calculating using XYEQ and the DSS reference image are taken to be their absolute coordinates on our reference image and all other science frames of the same field.

When choosing the 25 reference stars, it is important that they equally sample all regions of the image. This ensures that the plate solution will not be more heavily weighted for one spatial region of the CCD chip. Additionally, one of the reference stars should be relatively close to the center of the image. This star will serve as an origin for the plate solution. Using the IRAF routine HEDIT, the (x,y) and (RA,DEC) positions of this star, the latter in decimal degrees, are inserted into the header keywords CRPIX1, CRPIX2, CRVAL1, and CRVAL2, respectively. This is done for all images despite the fact that the relative (x,y) coordinates, CRPIX1 and CRPIX2, will be incorrect for all non-reference images, since those refer to the pixel position of the origin star in and only in the reference frame. The incorrect pixel positions are what allow for the calculation of the pixel shift of each image to the reference image in the next step.

Now the header keywords of the position of the origin star, in both pixel and equatorial coordinates, have been put in the header of all images. The next step is to run a custom script called POLYPLTSOL, written by Dr. Keivan Stassun, which takes a list of input images, registers them, and generates the files necessary for calculating image-specific plate solutions. The POLYPLTSOL routine takes, as inputs, the list of images to be registered, the ID of the reference star that serves as the origin, the non-DSS reference image, a table that contains only the pixel positions of all of the reference stars, and the table that contains the reference star IDS, pixel positions, and equatorial coordinates. Using these, it goes image by image and computes the pixel shift from each image to the reference image.

It does this by laying the input image on top of the reference image, multiplying each pair of pixels, and summing all of these values. This produces a specific number for that matching position, the magnitude of which represents the strength of the match for that given shift. This process of rastering the image is iterated numerous times, producing a value for all possible matching positions. One overlapping position will produce a value significantly greater than all others, corresponding to the best-fit pixel shift. This is a product of the fact that when the two images, input and reference, happen to be perfectly lined up, each pixel will be multiplied by its corresponding pixel on the

other image. Since each pixel of a star is multiplied by its counterpart in the reference image, a maximum raster value is found, and this value is the peak of the optimization function that denotes correct pixel shift. As this is completed for each image, POLYPLTSOL updates the CRPIX1 and CRPIX2 header keywords for each image, adding the pixel shift to the values already present to give the true pixel position of the origin reference star in that reference image.

Before proceeding to the next step, a visual check is necessary to ensure that the shifts found by POLYPLTSOL are accurate. A log file that contains the pixel shift of each input image is output by POLYPLTSOL. Using DS9, the IRAF-specific image viewing software, each image should be inspected and compared to the reference image to guarantee that the calculated shift is correct. This entails picking a common star and using the RIMEXAM command in IRAF to calculate the centroid of the star in both images. A quick subtraction of the two positions should yield values very near that of the shift. Once this has been checked for all input images, they are ready for the next phase, astrometric plate solution calculation.

II.II.II.II Astrometric Plate Solution

At this stage, all images have been registered and their headers contain the correct pixel and equatorial positions for the reference star that will serve as the origin for the plate solution. A custom script called RUNPLTSOL, written by Dr. Keivan Stassun, is used to run the IRAF routine PLTSOL on a set of images. This routine takes the list of images for which plate solutions are to be calculated and corresponding ref.imagename.dat files as inputs. These "dat" files contain the image-specific pixel positions for each of the 25 reference stars, the reference star IDs, and the equatorial coordinates for those stars. The PLTSOL routine looks in each image header and finds the CRPIX and CRVAL keywords, which, again, are the pixel and equatorial position of the reference star for that image. Using this in conjunction with the pixel and equatorial positions of all other reference stars, PLTSOL calculates a minimum set for that image, producing a plate solution.

The plate solution itself consists of two parts. The first part is the information about the origin of the plate solution, the CRPIX and CRVAL keywords, which were input prior to the running of RUNPLTSOL. The second part consists of a set of six transformation coefficients. The first, NAMDX1, specifies how the RA changes as a function of the x-coordinate of pixel position. The second, NAMDX2, indicates how the DEC changes as a function of the x-coordinate of pixel position. The third, NAMDX3, gives the (usually very small) offset of the origin specified by CRPIX/CRVAL relative to the true origin. The second set of coefficients, NAMDY1-3, provide the same information for the y-coordinate of pixel position. The first pair of coefficients should be roughly equal to the plate scale, 19.26667"/mm for our images, while the other coefficients should be roughly equal to zero because we expect the CCD to be well aligned, with rows running in the RA direction and columns running in the DEC direction.

The determination of the transformation coefficients is an interactive process through which five different plots are displayed for a given image. The first graphs the residuals of the fit in RA for each of the 25 reference stars as a function of x pixel

position. The second shows the residuals of the fit in RA as a function of y pixel position. The third and fourth plots show the residuals of the fit in DEC as a function of x and y pixel position, respectively. A fifth graph plots the residuals of the fit in RA versus the residuals of the fit in DEC. For each different plot, the user has the option to delete a star from the fit, recalculate the fit, and save the transformation coefficients as necessary. The residual of one of the absolute coordinates for a given reference star is the difference between the value of that coordinate as determined earlier using the DSS reference image and the value as calculated by starting with the origin reference star and applying the transformation coefficients for that pixel position. It is important to minimize residuals for all stars and to throw out those stars that have high residuals in both coordinates, as they skew the fit of the transformation coefficients. If all plots for a given image display acceptable residuals, then those coefficients are written into the image's header and the routine moves on to the next image. In this manner, the transformation coefficients are calculated for all images and saved in the headers, and the plate solutions are complete.

II.II.II.III PSF Photometry

At this stage, all images have been registered and their plate solutions have been calculated. Now they are ready to undergo PSF photometry, the process by which stellar magnitudes are extracted. Before this can happen, however, the photometry parameter files must be generated. This is accomplished via COMPPHOTPARS, an IDL routine written by Dr. Keivan Stassun. The routine calls for the list of files to be operated on as well as the readnoise, gain, and datamax value, which are all functions of the Y4K Cam CCD. The readnoise, measured in electrons, is the error in a given pixel's value. The gain is the ratio of how many electrons each unit of value for a pixel represents. Thus, if a pixel has a value of 10 counts and the CCD has a gain of 1.48, then that pixel received (10 * 1.48) = 14.8 electrons during the exposure. The datamax value represents the level of counts at which a pixel is saturated and begins to bleed into nearby pixels.

The COMPPHOTPARS routine takes these inputs and performs several tasks. It first calculates the full-width at half-maximum (FWHM) of all of the reference stars in a given image. It then calculates the average background sky value, the standard deviation of the sky background, and the lowest pixel value on the frame. For each image, the values of these photometric parameters, including the average FWHM of all the reference stars, are tabulated in a single output table, called fieldname.photpars. This table, then, contains all of the values for all photometric parameters for each image in the given field. It is used in the next step, during which the actual PSF photometry takes place.

The workhorse of this phase is a custom script written by Dr. Keivan Stassun, called AUTOPHOTPSF. This is an interactive routine that utilizes several IRAF packages and takes as inputs the list of images and the fieldname.photpars data file, which, as mentioned above, contains the photometric parameters. In a multistep interactive process, AUTOPHOTPSF goes through each image and calculates the magnitude of every source detection for that image.

In the first step, the IRAF routine DAOFIND locates every source that is five sigma above the background sky level. The (x,y) center, sharpness, and roundness of every detection are stored in a coordinate file. Then the magnitude of each star is

calculated via aperture photometry. The radius of the aperture to be used for a given image is taken from the FWHM value as read in from the fieldname.photpars file. Afterwards, a DS9 window is opened and the image is displayed. Using the IRAF TVMARK routine, all of the source detections found by DAOFIND are marked with points while the reference stars are marked with circles. With this information, the actual creation of the PSF can take place interactively.

In this phase, IRAF allows the user to cycle through several different graphs for a given reference star, deciding whether or not to reject it from what is called the Point Spread Function (PSF), which describes the average shape of a star on a given frame. The first plot shows a sort of physical map, with x and y pixel position plotted in the horizontal plane and the number of counts for the source in the z-direction. This plot can be rotated so as to view the entire spatial surroundings of the star and ensure that it is indeed isolated. A subsequent plot shows the radial profile of the star, with counts on the y-axis and radial pixel position on the x-axis. Such a plot, showing the values of all pixels within a certain user-specified radius of the centroid of the star, facilitates the detection of any bad pixels nearby or even within the star that may make it unsuitable as a PSF star. The third and final plot is akin to an elevation map, with x and y pixel position plotted in a plane and lines representing equally spaced levels of counts, thus showing the morphology of the magnitude of the star. This plot is useful to determine whether the star is circular. If so, then there would be a series of concentric circles. Any significant deviation from that pattern is cause for concern when considering that star as a PSF candidate. These three plots together allow the user to go through all reference stars and accept or reject them as contributors to the PSF.

Once PSF star selection is finished, it is time to construct the PSF and apply it to all images. The PSF is created by the IRAF routine called PSF. An average star shape as a function of (x,y) position on the CCD is generated by reading in the FWHM in the x and y direction for each reference star. This model is then scaled to match the peak of each star on the frame. Finally, photometry is performed with the PSF by the IRAF routine ALLSTAR. This entails integrating under the scaled PSF for a given star to obtain the total counts, which we can take to be a working relative magnitude for that star. Afterwards, a subtracted image is displayed in the DS9 window. At this point the user is able to check the quality of subtraction, which was performed by subtracting the star as it was modeled by the PSF from the star as it appears on the frame. As a useful check, the IRAF routine IMEXAM can generate radial profile plots of stars. Thus, plotting the radial profile of a star before the subtraction and overplotting the profile after the subtraction will give an indication of the quality of the subtraction. Iterating this process for several stars spaced across the image indicates whether the PSF subtraction is accurate across the entire frame.

If the subtraction is deemed acceptable, then IRAF creates two tables containing the astrometry and magnitudes of each of the stars. Finally, aperture photometry is once again performed, this time on the original and PSF-subtracted frame. A histogram displaying the difference in magnitude between the two aperture calculations is plotted as a final check on the quality of the PSF fitting. Once PSF photometry has been completed for a given frame, AUTOPHOTPSF begins with the next frame, exactly iterating these same steps. After AUTOPHOTPSF has been successfully run on all images, the magnitudes of all stars have been calculated, and it is time to create a working data cube.

The data cube for a certain field will contain the JD, magnitude, magnitude error, and (x,y) and (RA,DEC) position of every star in the given field. This is generated by successively running a series of IDL scripts written by Dr. Keivan Stassun. The astrometry file, containing the (RA,DEC) of every star on a given frame, and the magnitude file, containing the magnitude of every star on a given frame, are needed as inputs. The first IDL script to be run is called RDTABLEPSF, which takes the astrometry and magnitude files and initializes the data cube. Again, this data cube contains the magnitude, magnitude error, (x,y) center, and (RA,DEC) center of every source detection in every image.

At this point, any source detection is considered a unique one, exaggerating the total number of unique stars common to all frames for the given field. For example, even if a star has the exact same (x,y) and/or (RA,DEC) center on 100 frames, it will still be counted as 100 different detections on 100 different images, rather than a single unique detection located on a 100 different images. The subsequent IDL script, SORTSTARS, corrects for this and trims the data cube so as only to contain the number of unique detections. The SORTSTARS script takes the data cube produced by RDTABLEPSF, first sorting all of the stars and then cross-identifying stars across images. This ensures that in the output data cube each row corresponds to a single star. In order to effectively match stars, an appropriate matching radius is required. A 0.5" matching radius is used for the long exposure fields while a 1.0" matching radius is used for the short exposure fields. If, in a given frame, more than one star is found at the same position within the given matching radius, then that position is left blank for that image. As SORTSTARS runs, it outputs the IDs and (x,y) center of any stars that fell in the same radius on a given frame and so were thrown out.

Once SORTSTARS has created the data cube containing only unique source detections, it is time to pass the data cube through another filter, this one being the IDL script TRIMSTARS, written by Dr. Keivan Stassun. While the current data cube has the information for all unique and relatively isolated, at least within the user-defined matching radius, source detections, many of these detections occur on far too few frames to produce useful science. That is where TRIMSTARS comes into play. During the first pass, TRIMSTARS takes the data cube output by SORTSTARS and creates a new data data cube and an array of all of the "good" detections. A "good" detection is defined by a user-input keyword that indicates how many of the total frames a source must appear on to be included in the new data cube. This phase of the photometry requires two passes through TRIMSTARS.

For the first pass, the minimum frame appearance parameter is set to one. This will not remove any stars when creating the new data cube but will facilitate the creation of a histogram that plots the number of stars versus the number of frames in which they appear. An example histogram created during a first pass through TRIMSTARS is shown in Figure II.II.II.III.I. As shown, this plot displays the number of stars versus the number of detections and has two distinct horns, one at either end. The one on the left end, designating a small number of detections, is largely due to the stars found only in a single frame, and are most likely cosmic rays or other false detections. The other horn, at the far right end, represents those stars found in all frames. At this point a visual inspection of the histogram is necessary to determine the actual minimum number of frames a source must appear in to be included in the new data cube. We choose a value

Figure II.II.II.III.I: TRIMSTARS Histogram

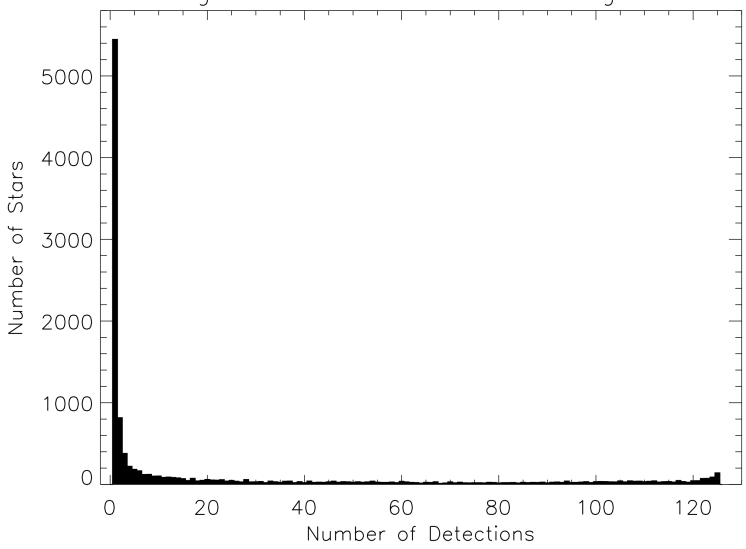

that represents about 60% of the total number of frames for a given field. Now the data cube output from SORTSTARS is passed through TRIMSTARS a second time, and all stars that don't appear in the minimum number of frames are thrown out, trimming the number of stars included in the final data cube. An example of the same TRIMSTARS histogram, this time with the stars below the detection cutoff, is shown in Figure II.II.II.III.II. This histogram more clearly shows the right horn of the graph, which

Figure II.II.II.III.II: TRIMSTARS Histogram

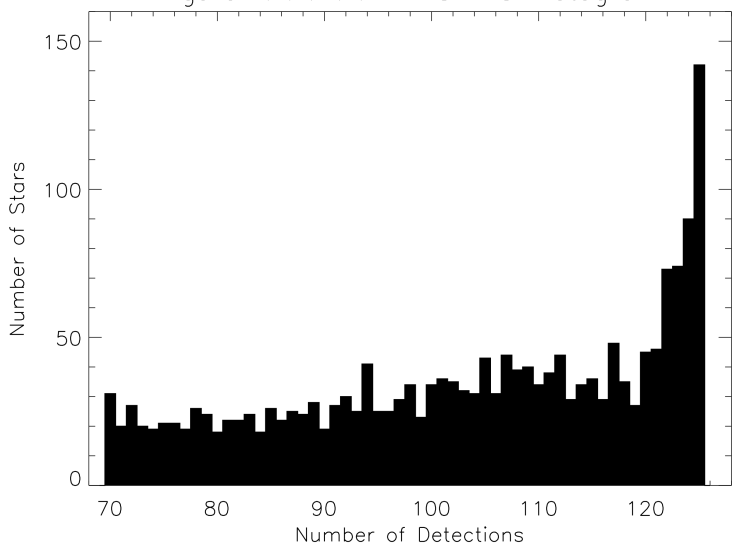

represents the number of stars found in all frames. After this second pass through TRIMSTARS, the data are ready for one final calibration.

II.II.II.IV Extrinsic Flux Normalization

The goal of this project is to find periodic photometrically variable stars and to use the properties of their light curves to test basic properties of stellar formation and evolution. As such, we are interested solely in magnitude variations that are intrinsic to the star, that are due to either the physics of the star itself or to the geometry of a multiple star system. Before light curves can be produced and such variations analyzed, it is necessary to remove what are called extrinsic flux variations. This refers to removal of dimming effects due to dust, clouds, or other contaminants in the Earth's atmosphere. The different types of calibration corrections mentioned in Section II.II.I only account for vagaries that are a function of the equipment, such as pixel throughput and zero-point variations. In order to remove extrinsic flux variations due to non-stellar processes, such as clouds, we use the method developed by Honeycutt (1992).

This algorithm executes stellar ensemble photometry on an inhomogeneous set of images using the least squares solution. Specifically, this involves deriving transformation coefficients and computing and solving matrices for the several tens of thousands of stars simultaneously. However, the large size of the data cube produced by TRIMSTARS precludes the executing of the Honeycutt method, compiled in the IDL routine HONEYDRV, on the entire data cube simultaneously with the CPU and memory constraints of a standard workstation. Therefore, the data cube for a given field must be subdivided. We accomplish this in IDL, splitting the TRIMSTARS data cube into four smaller data cubes corresponding to four quadrants of the given field. Then, rather than running HONEYDRV on the astronomy workstations, the data cube for each quadrant is submitted as a separate computational job to the Advanced Computing Center for Research and Education (ACCRE), Vanderbilt's supercomputing facility. Though increasing the number of sub-fields on which HONEYDRV needs to operate, this greatly expedites the overall process.

The HONEYDRV routine requires only the TRIMSTARS data cube as input. It goes through and compiles the magnitude of every star as it appears on every frame. In doing so it measures by how much the stars change in brightness from frame to frame. Then an arbitrary frame is picked as a reference frame, so that all other frames will have their magnitude shifted so as to equal this reference frame. A constant magnitude shift is applied to every other frame, and to all stars equally on each frame. After this has been iterated for all frames in the quadrant, HONEYDRV outputs five vectors. The largest is the data cube "difm", which contains the differential magnitude of each star (that made it through the earlier TRIMSTARS cut) for every frame on which that star appears. The vector "sigst" gives the standard deviation of the magnitude of every star. The vector "m0" represents the average magnitude of every star. The vector "em" indicates the magnitude shift that was applied to each frame as a whole by HONEYDRV, and the vector "sigim" gives the standard deviation of the applied magnitude shift. Now that HONEYDRV has been run on all four quadrants, the results are ready for the next phase: light curve production and analysis.

II.III Preliminary Light Curve Production

The focus of this phase is on the data cube output by TRIMSTARS and on the "difm" data cube output by HONEYDRV. The former contains the JDs and magnitude errors for all stars on all images while the latter contains the differential magnitudes for all stars. Before using these vectors to generate light curves, we need to match our catalog with that of Prisinzano, et al. (2005). We are currently interested solely in the PMS cluster members of NGC 6530. As such, rather than creating and sifting through several tens of thousands of light curves, we want to work only with those that correspond to verified cluster members. After reading in the positional data for the 828 stars of the Prisinzano, et al. (2005) catalog, we implement a positional matching search. Using a matching radius of 1.5" we find that 904 of our stars positionally match at least one star in the Prisinzano catalog. We obtain matches to 652 stars of the Prisinzano catalog, and have 252 stars that provide some stars in the Prisinzano catalog with multiple matches from our catalog. Since there is not a one-to-one correspondence for matches between catalogs, this induces an element of degeneracy in our matching routine, an issue that will be discussed in Section IV. Regardless, hereafter we will focus on the set of 904 stars, as they are guaranteed PMS cluster members.

Now that the JDs, magnitudes, and errors for all matched stars have been calculated and organized, the process of light curve production is relatively straightforward. The first step is to use the IDL routine PLOTERROR to plot the differential magnitude of a given star (again, we are focusing only on the stars that have been matched to the Prisinzano catalog) as a function of time, or in this case, JD, and to include the accompanying error bars. An example of such a plot is shown in Figure II.III.I. Visual inspection shows that since we are compiling data from two different summers, separated by almost a year, it is impossible to visually do anything useful with

Figure II.III.I: Preliminary Lightcurve

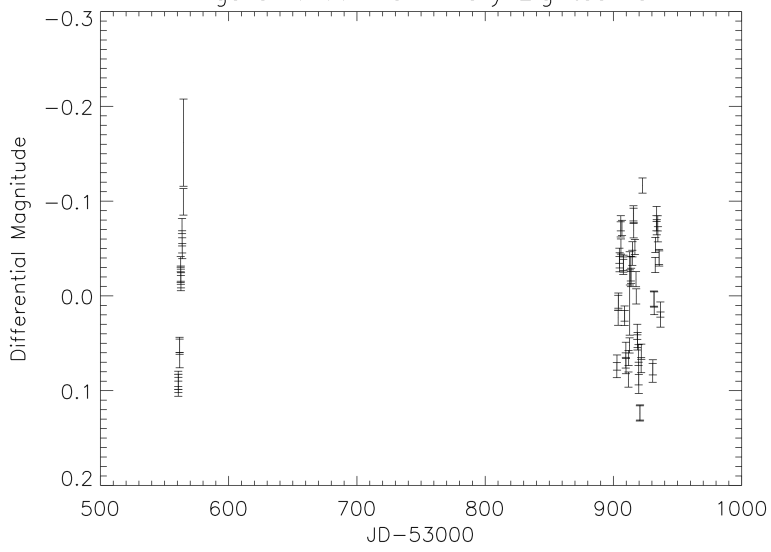

such a plot. Thus, the data for every star is split up into its two component data sets, one from the summer of 2005 and ther other from the summer of 2006. Figures II.III.II and II.III.III show the same light curve after it has been separated as such. After this is finished for every star we can sift through them and look for particularly interesting light curves. While useful in its own right, this phase of visual inspection is but a preliminary one. The next step will methodically and mathematically search for periodicity in the light curves of every star.

Figure II.III.II: Preliminary Lightcurve, 2005 Data

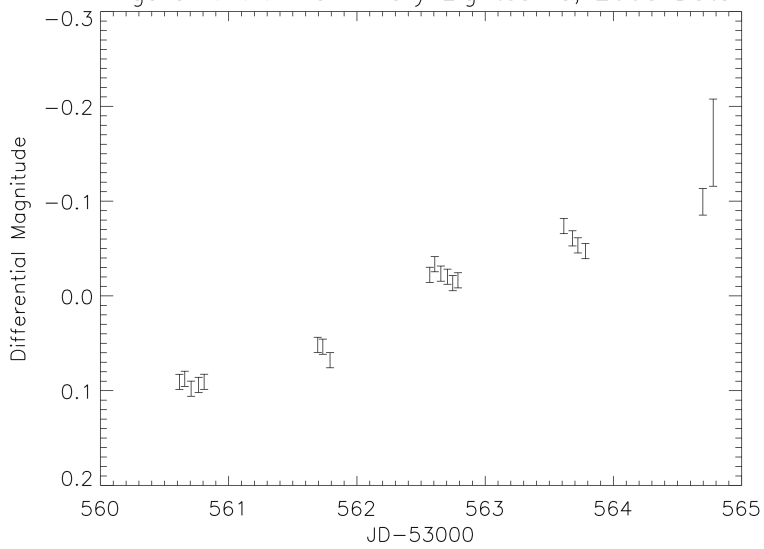

Figure II.III.III: Preliminary Lightcurve, 2006 Data

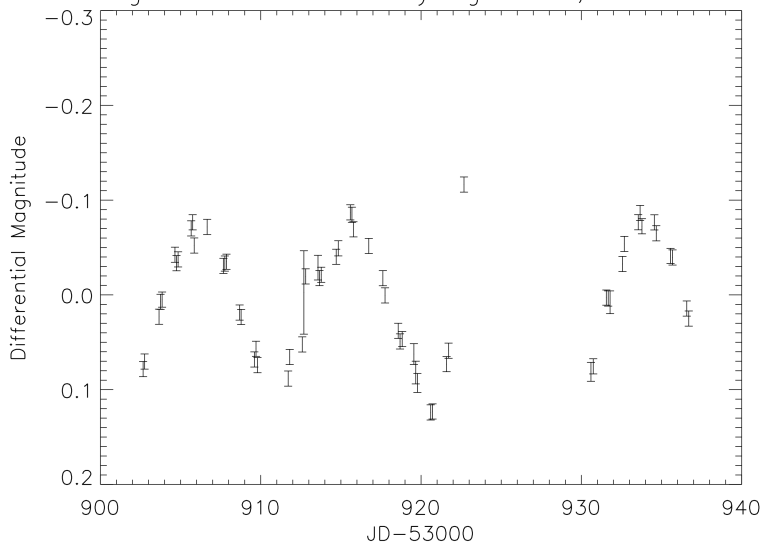

II.IV Periodicity Search

We use the Scargle periodogram technique to search for periodicity in the light curves of the 904 matched stars. The entire process is encapsulated in the IDL routines MINIPERSEARCH, PSINSPEC, P3DSPEC, and FAPCALC, all written by Dr. Keivan Stassun. This method allows the user to specify the upper and lower bound of the frequency (or period) space to be searched. A third parameter, the resolution, indicates the number of spectrum points to be searched within the given frequency window. Also input are the vectors containing the differential magnitude and JDs of every measurement of every star. The PSINSPEC routine computes the amplitude and phase of the best-fit sine function at each trial frequency for a given star's light curve. Then MINIPERSEARCH extracts the period of the sine function with the strongest and most robust fit.

After that, FAPCALC generates 100 random light curves and calls P3DSPEC to similarly compute a power spectrum for each of those light curves. Thus, for each of the 100 random light curves, the amplitude and phase of the best-fit sine function at each trial frequency is computed. Then, the peak in the power spectrum for each of these random light curves is calculated. Finally, the strongest of all of these 100 peaks is extracted, and this is what is referred to as the false-alarm probability (FAP). The FAP indicates the one-percent probability that the strength of the fit for the actual light curve could be randomly generated. Figure II.IV.I shows an example power spectrum for a real light curve, plotting power versus period for all spectrum points. The period calculated for this star, corresponding to the period of the sine curve with the highest power, is 0.6523 days, and the relative strength of that fit is indicated by the towering peak at the left. Figure

Figure II.IV.I: Power Spectrum

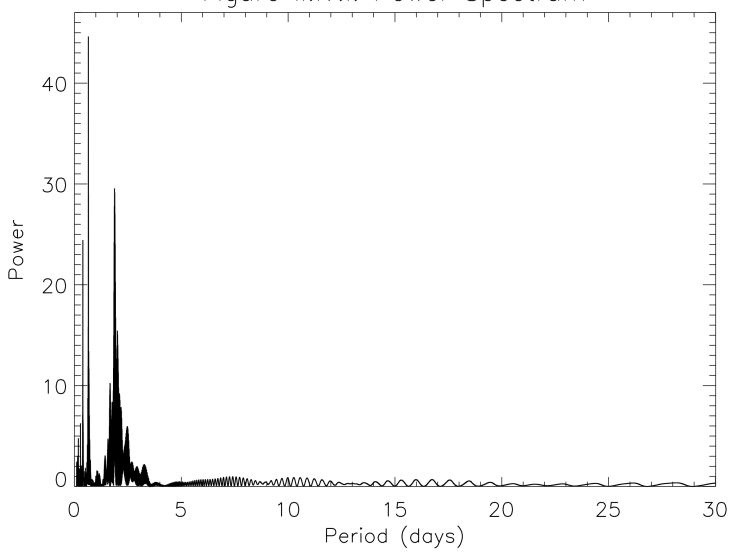

II.IV.II zooms in to a smaller period window to show more of the structure of the power spectrum. Furthermore, the FAP value is overplotted in red, to give a visual comparison of the strength of the peak in the real power spectrum to the FAP. As shown, this is a star for which the power is high relative to the FAP, indicating that this is very likely a significant period.

As shown, however, there are three peaks in the power spectrum great than the FAP. The peak at ~1.9 days corresponds to the beat frequency between the true period of the star, ~0.65 days, and the frequency of the measurements. Since the earth rotates daily, we are only able to image our region of interest with a roughly daily cadence. There is a series of peaks to the left of the true peak at ~0.65 days, decreasing in power with increasing frequency. These peaks are due to a phenomenon known as aliasing, by which integer multiples of the real frequency also exhibit significant strength in the power spectrum. The actual period of the star, then, is still the strongest peak in the power spectrum, residing at ~0.65 days.

Figure II.IV.II: Power Spectrum with FAP

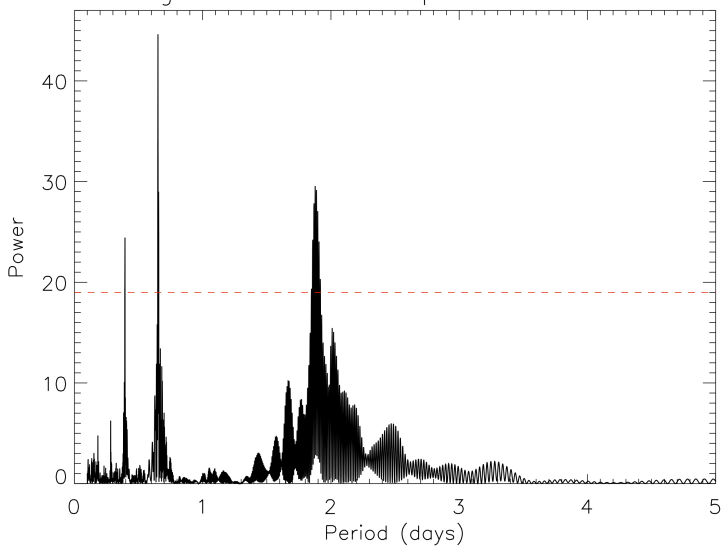

The FAP value is sent to MINIPERSEARCH, along with the peak in the power spectrum for the actual light curve of the star and the period to which that peak corresponds. This is iterated for every star, and compiled and output by MINIPERSEARCH. The first column contains our index for the star, the second the ID given by Prisinzano, et al. (2005), the third is the period of the best-fit sine function, the fourth the false-alarm probability, the fifth the peak of the power spectrum for the best-fit sine function, and the sixth the number of detections for that star. As discussed in the next section, these values allow us to locate stars with statistically significant rotation periods and to study them in further detail.

III. Results

The period searching routine finds periods for the light curves of all of the stars. However, to determine whether a period is significant and plausible, we require that the Power be great than or equal to the FAP for a given star. With this criterion in hand, we find significant rotation periods for 251 of the 904 total stars matched to the Prisinzano, et al. (2005) catalog. Of these 251 stars with significant periods, there are 223 unique matches in the Prisinzano, et al. (2005) catalog. The remaining 28 stars corresponding to double and occasional triple matches from our catalog, a degeneracy akin to the one mentioned earlier. Upon visual inspection of all light curves, sixteen eclipsing binary candidates have also been identified. Such a catalog of significant rotation periods and eclipsing binary candidates provides an excellent selection sample to begin to explore our scientific goals. The array of significant rotation periods for PMS cluster members allows us to study the early stages of the evolution of stellar angular momentum. The assortment of eclipsing binary candidates facilitates the gathering of further information regarding early phases of stellar evolution. These two questions will occupy the remainder of our focus.

III.I Stellar Rotation Periods

Table III.I.I shows the output table of the Scargle period search for a single quadrant of one field, organized by increasing period. Table III.I.II shows the same table after all insignificant periods, those with FAP greater than Power, have been removed. We placed the additional constraint that the period must be less than 0.95 days or greater than 1.05 days. This was done so as to exclude all stars that, even with significant Power/FAP ratios, we still believe to have spurious periods. Any periods that are an integer multiple of one day, and most prominently those very near exactly one day, suffer from being on the order of the frequency of nightly observations. Thus, as an initial constraint we threw out all stars that didn't satisfy the aforementioned period criterion.

Appendix A contains the light curves for five stars with statistically significant rotation periods. Each plot contains data from both sets, the summer of 2005 and the summer of 2006, with the former in green and latter in red. The y-axis shows the differential magnitude of the stars with error bars. For each star, the differential magnitude at a given JD is calculated by subtracting the average magnitude of that star across all frames from the star's magnitude as measured on that frame. The x-axis displays phase rather than strict JD. The phase is calculated by computing the modulus of the JD of a given data point over the period found by the Scargle technique and dividing that value by the period itself. Now, rather than extending from the JD of the first observation to the JD of the last observation, the domain is [0,1]. Furthermore, for visual clarity we copy the data points into a second phase, so that the domain is [0,2] in phase space. It is important to remember that all of the data points within each of the two phases are identical, they are just duplicated for the sake of convenience.

Table III.I.I: Output of minipersearch.pro IDL routine

Resolution = 30,000, Permin = 0.1d, Permax = 30d

Index	ID	Period	FAP	Power	N
5	32864	0.1018	19.5	6.77	103
120	24368	0.1018	15.9	7.95	79
11	29873	0.1105	21.7	6.08	84
2	34984	0.1182	18.7	5.91	70
152	21437	0.1561	18.0	6.97	101
91	27470	0.1874	12.1	45.09	108
86	28743	0.2428	17.5	6.22	111
71	23296	0.4972	18.6	9.35	80
105	23295	0.5308	18.2	9.73	77
146	21025	0.5374	20.2	14.29	90
112	21654	0.6366	18.6	14.94	73
31	25374	0.6523	19.0	45.09	111
96	26832	0.6834	21.0	36.18	83
27	25964	0.7779	19.0	27.21	83
151	25571	0.7975	15.4	18.80	95
37	22050	0.8005	18.5	41.38	106
45	30975	0.8058	19.7	17.56	88
87	28512	0.8330	16.8	17.02	90
142	23459	0.8607	17.4	23.90	74
43	35380	0.8782	19.3	10.92	105
36	22808	0.8829	23.0	32.57	102
126	21348	0.9006	27.8	23.27	107
57	26466	0.9402	24.3	8.36	96
32	24932	0.9769	26.2	17.86	95
33	24837	0.9839	19.9	41.59	89
134	23284	0.9894	22.1	15.54	75
80	32258	1.0009	18.0	13.42	106
61	25897	1.0069	24.7	30.26	87
69	23856	1.0096	21.8	22.54	76
25	26138	1.0100	20.3	19.18	110
127	19726	1.0106	21.5	30.90	73
110	22047	1.0158	15.8	6.79	74
141	25071	1.0425	18.5	23.16	105
122	22010	1.0893	20.1	7.48	83
1	30283	1.1638	28.1	4.06	105
159	27530	1.1872	21.1	17.73	70
161	27530	1.1872	15.8	19.28	72
102	24121	1.2131	21.0	15.98	77
115	29944	1.2209	21.7	7.98	94
54	27111	1.2791	21.4	19.20	89
40	36379	1.2796	21.5	30.64	80
140	28352	1.2989	25.1	49.57	113

95	26918	1.3661	20.5	29.23	85
144	21369	1.5184	25.8	29.68	103
101	24293	1.5238	22.8	29.22	78
51	28138	1.5473	22.9	26.16	96
155	27805	1.5748	19.6	18.54	82
7	32276	1.6163	22.4	11.98	84
4	33362	1.6409	27.5	35.91	116
98	25346	1.6436	21.0	11.40	74
35	23688	1.7207	25.1	33.03	99
157	25460	1.7236	20.3	11.81	79
97	26297	1.8129	25.3	29.61	86
160	28700	1.9453	21.2	19.79	98
148	24720	1.9760	21.7	18.03	79
107	22930	1.9969	17.4	11.30	75
9	30517	2.4112	32.1	44.74	118
145	21103	2.4485	17.5	9.12	76
13	29815	2.5182	24.2	30.02	89
14	29683	2.7109	22.8	18.19	102
153	24774	2.9045	19.2	8.97	81
116	28541	3.1021	25.8	28.06	113
108	22687	3.1841	22.4	12.21	97
89	27870	3.2250	23.2	27.65	90
58	26427	3.3211	24.5	13.74	110
130	25568	3.3846	27.2	17.67	89
53	27121	3.5440	29.4	35.77	112
82	30697	3.6559	20.6	10.63	91
56	26667	3.6648	22.5	33.35	82
65	25120	3.6873	19.0	22.18	83
70	23643	3.7423	21.0	13.73	97
143	23122	3.7516	24.1	45.46	98
154	22314	3.7657	18.1	12.49	78
163	30697	3.7704	20.5	14.61	96
137	21366	3.9176	18.7	17.54	90
114	31409	4.2736	25.3	32.14	87
150	20620	4.3041	19.5	16.18	72
165	23651	4.4179	25.2	26.04	103
147	25505	4.4439	25.5	36.00	91
162	23651	4.4703	28.6	24.68	97
113	31545	4.5583	25.8	29.53	88
66	24784	4.6427	26.9	20.91	109
17	28928	4.8212	20.3	18.36	84
77	36784	4.8838	32.0	51.00	118
20	27887	5.0056	23.7	11.92	94
22	27078	5.0731	24.4	35.27	103
99	25270	5.1075	24.7	16.61	105
76	21066	5.2227	18.1	9.98	74
44	32594	5.2409	23.6	20.57	106
128	29528	5.2409	23.5	37.13	84
136	22455	5.2500	25.2	19.87	108

12	29848	5.3056	20.4	17.41	81
34	23886	5.4794	21.1	10.90	111
111	21812	5.5196	23.5	13.33	107
63	25540	5.6544	17.8	15.36	74
84	29014	5.7080	30.1	22.24	118
79	33415	5.9448	24.7	23.45	95
10	30269	5.9802	28.9	16.93	106
60	25944	6.0402	23.2	22.35	84
26	26045	6.1892	22.3	29.89	83
85	28903	6.2665	19.2	29.11	81
135	22515	6.2665	17.6	5.84	76
46	30830	6.4965	29.3	38.85	109
129	26991	6.4965	24.0	14.40	104
28	25906	6.5105	24.1	25.74	88
158	23651	6.6106	24.9	22.42	89
156	21771	6.6544	19.5	16.89	73
18	28502	6.8049	34.6	42.39	111
49	29462	7.0935	31.1	36.95	113
119	24596	7.1610	30.8	42.83	101
59	26202	7.1953	22.9	16.83	84
93	27185	7.4629	22.2	36.20	83
30	25684	7.5376	20.3	20.48	84
104	23805	7.5376	20.7	36.72	86
106	23073	7.5565	20.1	32.72	80
78	36232	7.6332	29.0	34.75	114
38	20559	7.6526	19.8	26.48	74
133	23419	7.7114	22.1	23.31	87
125	21488	7.9142	22.6	19.27	77
0	30427	7.9771	23.3	11.98	90
72	22761	7.9983	18.4	24.60	82
131	25513	8.2166	23.0	18.05	82
73	22030	8.3767	23.2	18.34	101
52	27255	8.4949	24.5	27.99	88
6	32646	8.7163	26.2	26.01	97
47	30020	8.7163	26.5	43.89	102
42	35460	8.7671	23.1	21.41	99
50	28967	8.8966	21.3	36.58	82
149	22509	8.9230	23.4	14.19	96
88	28399	8.9762	24.8	26.64	90
3	34304	9.0301	19.1	8.84	84
103	23945	9.2238	21.0	36.35	83
41	35944	9.4260	24.3	22.57	94
117	28087	9.4556	29.0	23.13	105
19	28153	9.4854	23.8	31.25	84
81	31912	9.6993	24.1	12.40	96
90	27558	9.9232	23.2	16.45	88
94	27090	10.0223	28.8	25.65	104
68	24149	10.0895	26.1	20.84	92
123	21791	10.2614	19.2	20.03	77

24	26328	10.3675	31.3	14.25	116
62	25554	10.4394	22.7	26.82	80
132	23677	10.6991	26.3	20.59	99
48	29698	10.7757	18.7	8.97	110
100	25249	10.9721	23.5	14.87	115
124	21719	11.8817	21.3	9.76	85
8	31634	12.4210	28.7	27.94	111
29	25848	12.4725	23.5	25.23	82
64	25523	12.9001	25.7	27.35	101
15	29284	12.9556	26.4	41.90	113
23	26778	13.4777	27.0	19.17	111
118	26301	13.4777	17.6	17.91	73
74	21912	13.8498	28.8	10.49	107
109	22324	14.0436	27.2	19.65	98
39	36910	14.9504	22.1	19.37	85
21	27217	17.3655	28.1	28.27	115
164	21086	17.7757	21.7	25.50	72
83	30700	17.9881	20.9	15.01	82
139	20366	19.7594	21.7	21.38	80
55	27091	23.8259	26.0	28.74	104
138	21339	24.4055	18.7	22.14	78
67	24459	25.8740	21.2	17.47	84
16	29085	27.7846	20.2	24.36	81
75	21246	28.0435	19.0	10.49	83
92	27317	28.0435	24.2	24.69	85
121	24288	30.0000	21.8	24.47	84

Table III.I.II: Period search data for stars with Power > FAP

Resolution = 30,000, Permin = 0.1d, Permax = 30d

Index	ID	Period	FAP	Power	N
91	27470	0.1874	12.1	45.09	108
31	25374	0.6523	19.0	45.09	111
96	26832	0.6834	21.0	36.18	83
27	25964	0.7779	19.0	27.21	83
151	25571	0.7975	15.4	18.80	95
37	22050	0.8005	18.5	41.38	106
87	28512	0.8330	16.8	17.02	90
142	23459	0.8607	17.4	23.90	74
36	22808	0.8829	23.0	32.57	102
161	27530	1.1872	15.8	19.28	72
40	36379	1.2796	21.5	30.64	80
140	28352	1.2989	25.1	49.57	113
95	26918	1.3661	20.5	29.23	85
144	21369	1.5184	25.8	29.68	103
101	24293	1.5238	22.8	29.22	78
51	28138	1.5473	22.9	26.16	96
4	33362	1.6409	27.5	35.91	116
35	23688	1.7207	25.1	33.03	99
97	26297	1.8129	25.3	29.61	86
9	30517	2.4112	32.1	44.74	118
13	29815	2.5182	24.2	30.02	89
116	28541	3.1021	25.8	28.06	113
89	27870	3.2250	23.2	27.65	90
53	27121	3.5440	29.4	35.77	112
56	26667	3.6648	22.5	33.35	82
65	25120	3.6873	19.0	22.18	83
143	23122	3.7516	24.1	45.46	98
114	31409	4.2736	25.3	32.14	87
165	23651	4.4179	25.2	26.04	103
147	25505	4.4439	25.5	36.00	91
113	31545	4.5583	25.8	29.53	88
77	36784	4.8838	32.0	51.00	118
22	27078	5.0731	24.4	35.27	103
128	29528	5.2409	23.5	37.13	84
26	26045	6.1892	22.3	29.89	83
85	28903	6.2665	19.2	29.11	81
46	30830	6.4965	29.3	38.85	109
28	25906	6.5105	24.1	25.74	88
18	28502	6.8049	34.6	42.39	111
49	29462	7.0935	31.1	36.95	113
119	24596	7.1610	30.8	42.83	101
93	27185	7.4629	22.2	36.20	83

30	25684	7.5376	20.3	20.48	84
104	23805	7.5376	20.7	36.72	86
106	23073	7.5565	20.1	32.72	80
78	36232	7.6332	29.0	34.75	114
38	20559	7.6526	19.8	26.48	74
133	23419	7.7114	22.1	23.31	87
72	22761	7.9983	18.4	24.60	82
52	27255	8.4949	24.5	27.99	88
47	30020	8.7163	26.5	43.89	102
50	28967	8.8966	21.3	36.58	82
88	28399	8.9762	24.8	26.64	90
103	23945	9.2238	21.0	36.35	83
19	28153	9.4854	23.8	31.25	84
123	21791	10.2614	19.2	20.03	77
62	25554	10.4394	22.7	26.82	80
29	25848	12.4725	23.5	25.23	82
64	25523	12.9001	25.7	27.35	101
15	29284	12.9556	26.4	41.90	113
118	26301	13.4777	17.6	17.91	73
21	27217	17.3655	28.1	28.27	115
164	21086	17.7757	21.7	25.50	72
55	27091	23.8259	26.0	28.74	104
138	21339	24.4055	18.7	22.14	78
16	29085	27.7846	20.2	24.36	81
92	27317	28.0435	24.2	24.69	85
121	24288	30.0000	21.8	24.47	84

III.II Eclipsing Binary Candidates

Of the 904 stars in our catalog that we matched with the Prisinzano catalog, we identify sixteen eclipsing binary candidates. These are stars whose light curves appear to resemble the periodic signal indicative of such a system. Two such light curves are shown in Figures III.II.I and III.II.II. There are several important characteristics to note about these light curves. The first and perhaps most visually apparent is the prominence of two dips in brightness. These correspond to the phases of the rotation during which one of the component stars is eclipsing the other, an opportunity provided by the geometry of the system. The second is the significant dimming of the system throughout the dips. In Figure III.II.I the total magnitude drop is on the order of 0.5 magnitudes and Figure III.II.II shows a magnitude drop of approximately 1.0 magnitudes. These are relatively large drops in brightness, particularly when compared to the amplitude of the rotation period light curves, which will be examined in further detail in Section IV.

Figure III.II.I: Eclipsing Binary Candidate

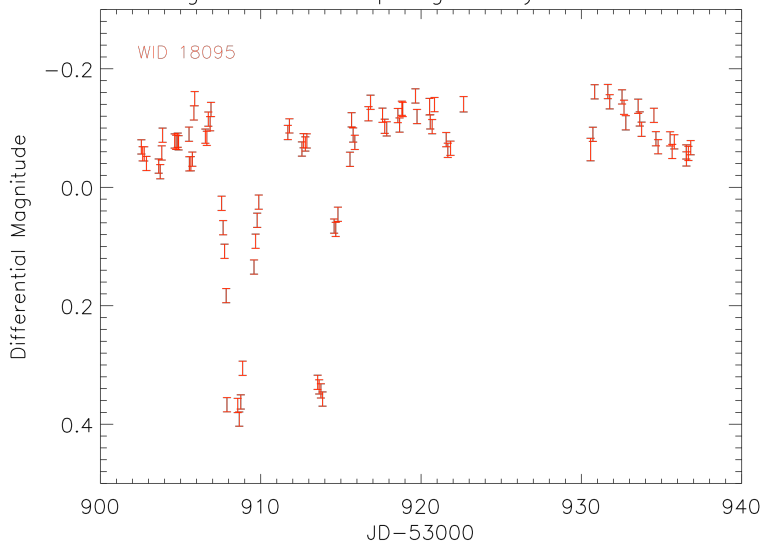

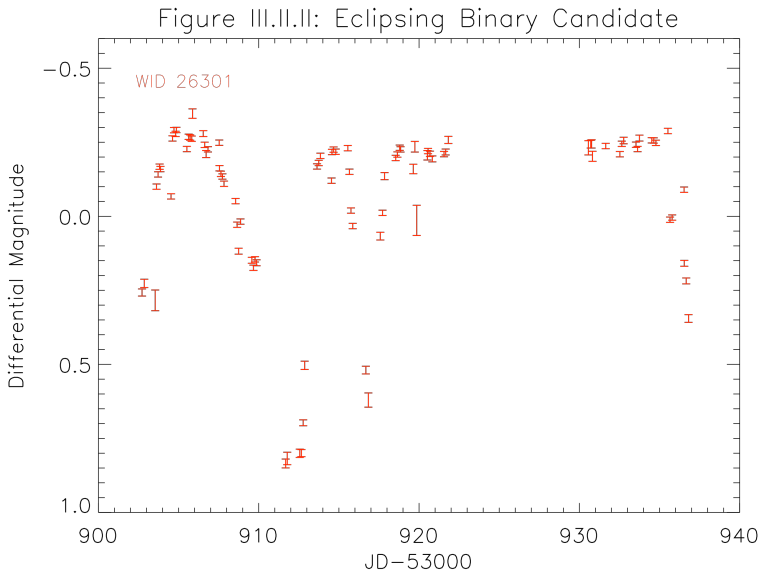

Currently we are at the incipient stage of eclipsing binary candidate identification. The next phase is to expand the sample of eclipsing binary candidates by doing a rigorous mathematical periodicity search tailored to the signature light curve structure of such a system. Once a final catalog is compiled, we will gather further photometric and spectroscopic data. The former will allow us to refine the period measurement and measure the ratio of surface temperatures of the two stars. The latter will allow us to constrain the stellar masses and compute orbital elements such as the eccentricity and semi-major axis. An example of a refined light curve is shown in Figure III.II.III.

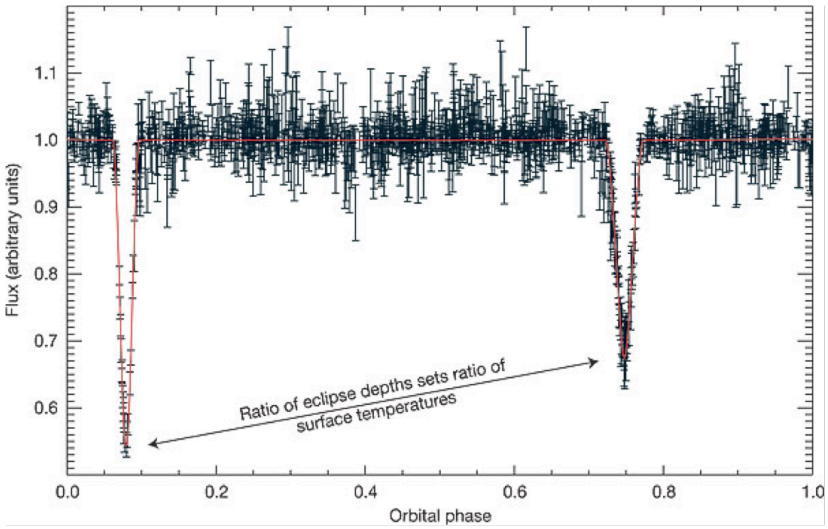

Figure III.II.III: A light curve of a known eclipsing binary system found by Stassun et al. (2006)

IV. Discussion

We will first analyze the results of our periodicity search among young PMS cluster members of NGC 6530. Figure IV.I shows a period histogram for all unique Prisinzano-matched stars, using a bin size of 1.0 days. The shortest significant period we

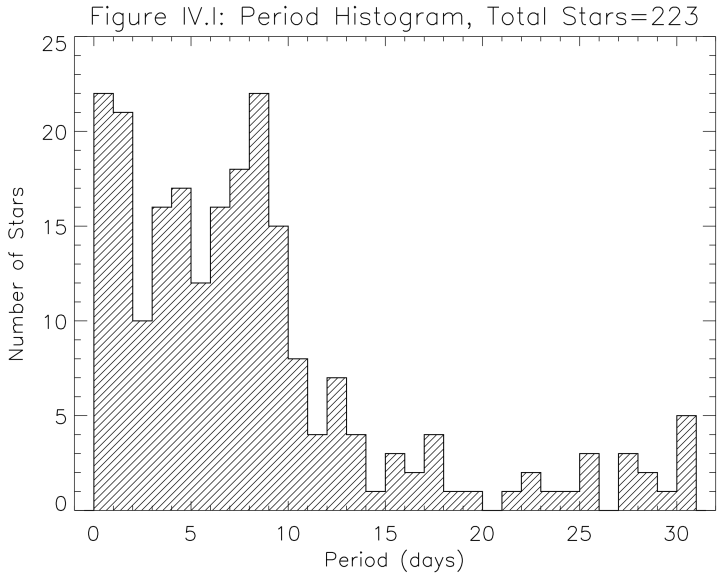

find is 0.1035 days. We find five unique stars with a period of 30.0000 days. While these periods are indeed statistically significant according to our criterion, we believe them to be somewhat dubious because they are the limit of our period search. However, we do believe those periods to be the correct order of magnitude. Further investigation is needed to identify the true characteristics of those light curves. The bulk of the periods, 169 out of 223, are within the 0.1 – 10.0 day range. Figure IV.II shows the same histogram with a bin size of 0.5 days to reveal the structure of the period distribution, which we proceed to compare to the literature.

Herbst et al. (2006) compiled a review of the rotation data for low-mass stars, and we will draw on it heavily here. Herbst et al. (2006) report that rotation periods have been measured to 1% for approximately 1700 low-mass PMS stars. The period distribution of these stars ranges from ~0.6 days to ~20 days within the mass range $0.4\ M_{sun} < M < 1.5\ M_{sun}$. This is comparable to the mass range reported by Prisinzano et al. (2006) for NGC 6530, $0.25\ M_{sun} < M < 4.0\ M_{sun}$, and so it is useful to compare the results. Data from the ONC exhibit bimodal peaks at 2 and 8 days while data from NGC 2264 exhibit bimodal peaks at 1 and 4 days. Our own data, as elucidated by the smaller bin size in Figure IV.II, appear almost trimodal, with peaks at ~1, 4, and 8 days. Such structure in the histogram is perhaps indicative of different angular momentum properties for different populations of stars. Herbst et al. (2006) notes that rotation rates of PMS

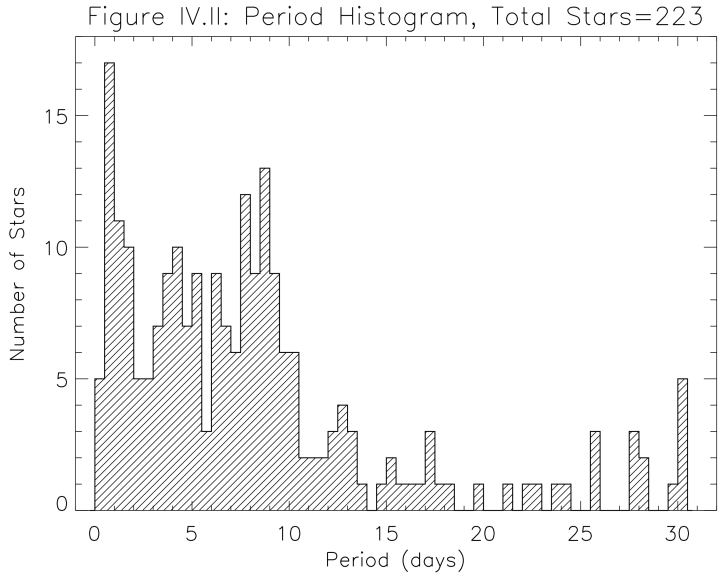

stars vary as a function of mass. This is a question we plan on addressing in order to further understand the evolution of angular momentum with time and in different mass regimes.

In looking at our histogram, it is also apparent that there is a distinct drop-off in periods shorter than ~0.5 days. This most likely results from the breakup velocities corresponding to stars with these properties. We begin analyzing this by deriving the breakup velocity from first principles. The breakup velocity is that velocity at which the rotation rate of the star at the equator is great enough so as to cause mass to be flung off. Start, then, by setting the centripetal force at the equator equal to the gravitational force:

$$F_c = F_g$$

$$\frac{m v_{br}^{\,2}}{R_*} = \frac{G M_* m}{R_*^{\,2}}$$

$$v_{br} = \sqrt{\frac{G M_*}{R_*}}$$

We will calculate the breakup velocity for a representative star using fiducial values of 1.0 M_{sun} and 2.5 R_{sun} for mass and radius. This gives a breakup velocity of ~$2.76 \bullet 10^5$ m/s. Now we use the following relation between rotational velocity and period to calculate the shortest possible period for our sample star:

$$v = \frac{2\pi R_*}{P}$$

$$P = \frac{2\pi R_*}{v_{br}}$$

Performing the calculation gives a shortest possible period of ~0.49 days. While this has been only a cursory derivation, ignoring the possibility of non-equatorial star spots, for only one specific star, it gives a shortest period on the order of what we find to be the case from our histogram.

We will further investigate the period distribution and characteristics of cluster members of NGC 6530. This will involve a more in-depth analysis of the structure of the period histogram and how it compares to the data for other PMS stars. Furthermore, we will look for clues that elucidate the evolution of angular momentum for young PMS stars, and as a function of stellar properties such as mass and presence of a circumstellar disk.

V. Summary

We report time-series CCD I-band photometry for the pre-main-sequence cluster NGC 6530, located within the Lagoon Nebula. We find approximately 1,000 of these stars to be bona fide members of the cluster with masses in the range 0.25-4.0 M_{sun}, assuming a distance of 1.25 kpc to the cluster. Our goals are to measure rotation periods for these stars and to identify eclipsing binary candidates. Here we present light curves of the 223 stars in our sample found by us to be periodically variable, and we present the distribution of the stellar rotation periods derived from these light curves. We also present 16 potential eclipsing binary star systems that, through follow-up work, will provide direct measurements of the masses and radii of the stars for testing of stellar evolutionary models.

References

- Damiani, F., Flaccomio, E., Micela, G., Sciortino, S., Harnden, Jr., F. R., & Murray, S. S. 2004, The Astrophysical Journal, 608, 781 "A Deep *Chandra* X-Ray Observation of the Rich Young Cluster NGC 6530"
- Damiani, F., Prisinzano, L., Micela, G., & Sciortino, S. 2006, Astronomy and Astrophysics, 459, 477 "The rich young cluster NGC 6530: a combined X-ray-optical-infrared study"
- Herbst, W., Eisloeffel, J., Mundt, R., Scholz, A. 2006 Review Chapter for Protostars and Planets V, "The Rotation of Young Low-Mass Stars and Brown Dwarfs"
- Honeycutt, R. K. 1992, Publications of the Astronomical Society of the Pacific, 104, 435 "CCD Ensemble Photometry on an Inhomogeneous Set of Exposures"
- Prisinzano, L., Damiani, F., Micela, G., & Sciortino, S. 2005, Astronomy and Astrophysics, 430, 941 "The star formation region NGC 6530: Distance, ages, and initial mass function"
- Stassun, K. G., Mathieu, R. D., & Valenti, J. A. 2006, Nature, 440 "Discovery of Two Young Brown Dwarfs in an Eclipsing Binary System"

Appendix A

The following pages contain the light curves for five sample stars of the 223 members of cluster NGC 6530 that we find to have statistically significant rotation periods. This selection is representative of the range of the period distribution.

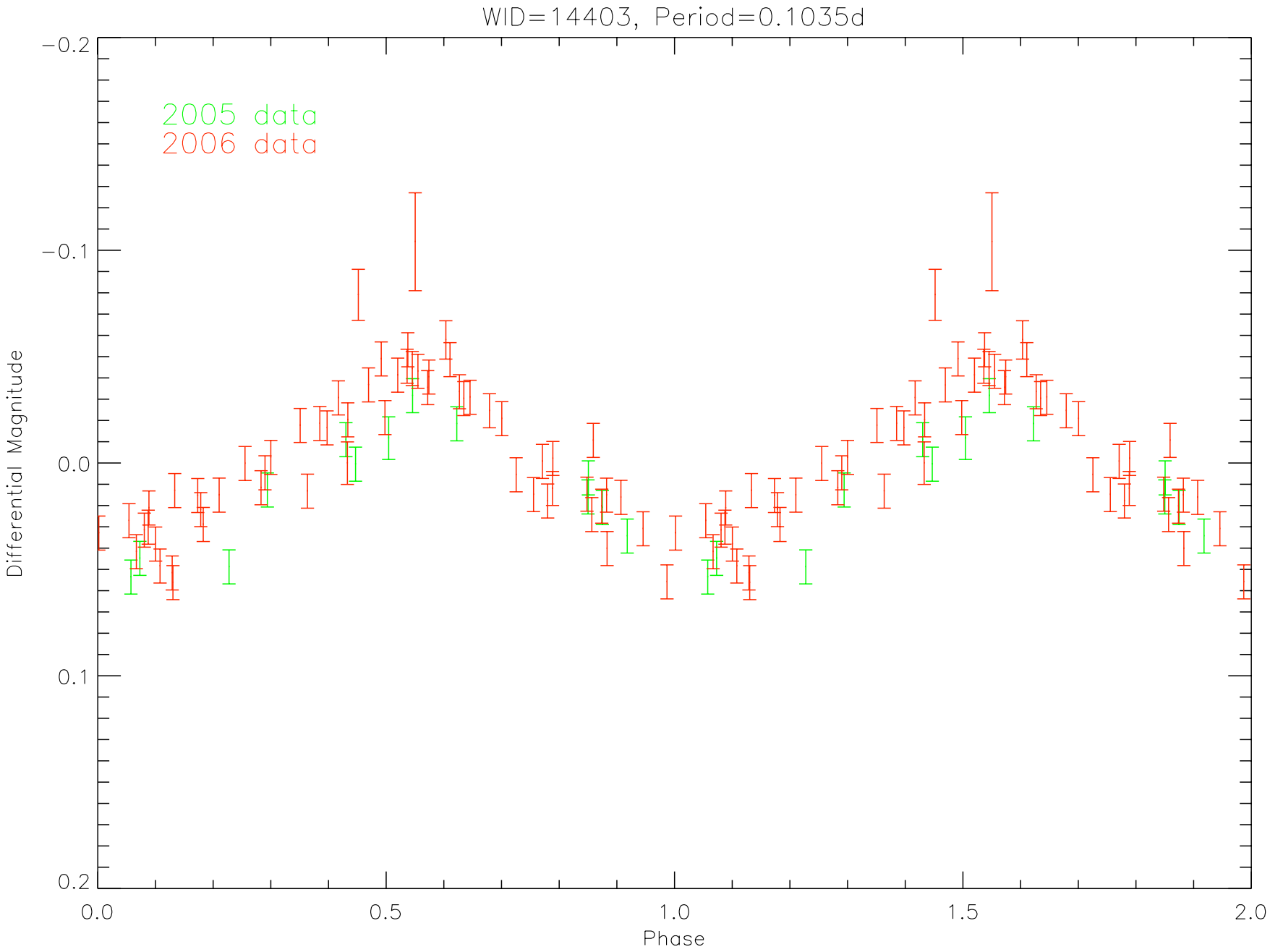
WID=14403, Period=0.1035d
2005 data
2006 data
Differential Magnitude
−0.2
−0.1
0.0
0.1
0.2
0.0
0.5
1.0
1.5
2.0
Phase

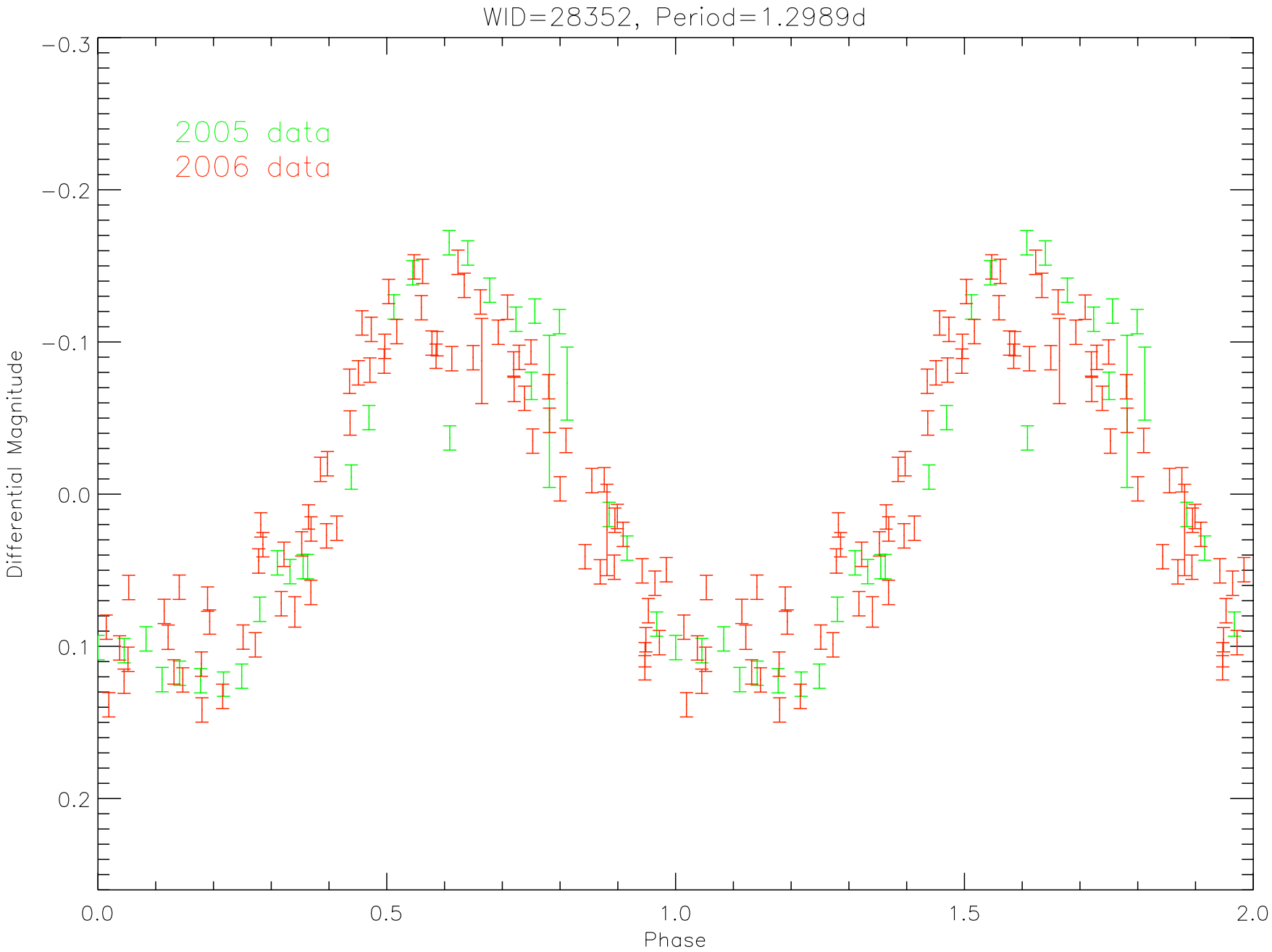
WID=28352, Period=1.2989d
2005 data
2006 data
Differential Magnitude
−0.3
−0.2
−0.1
0.0
0.1
0.2
0.0
0.5
1.0
1.5
2.0
Phase

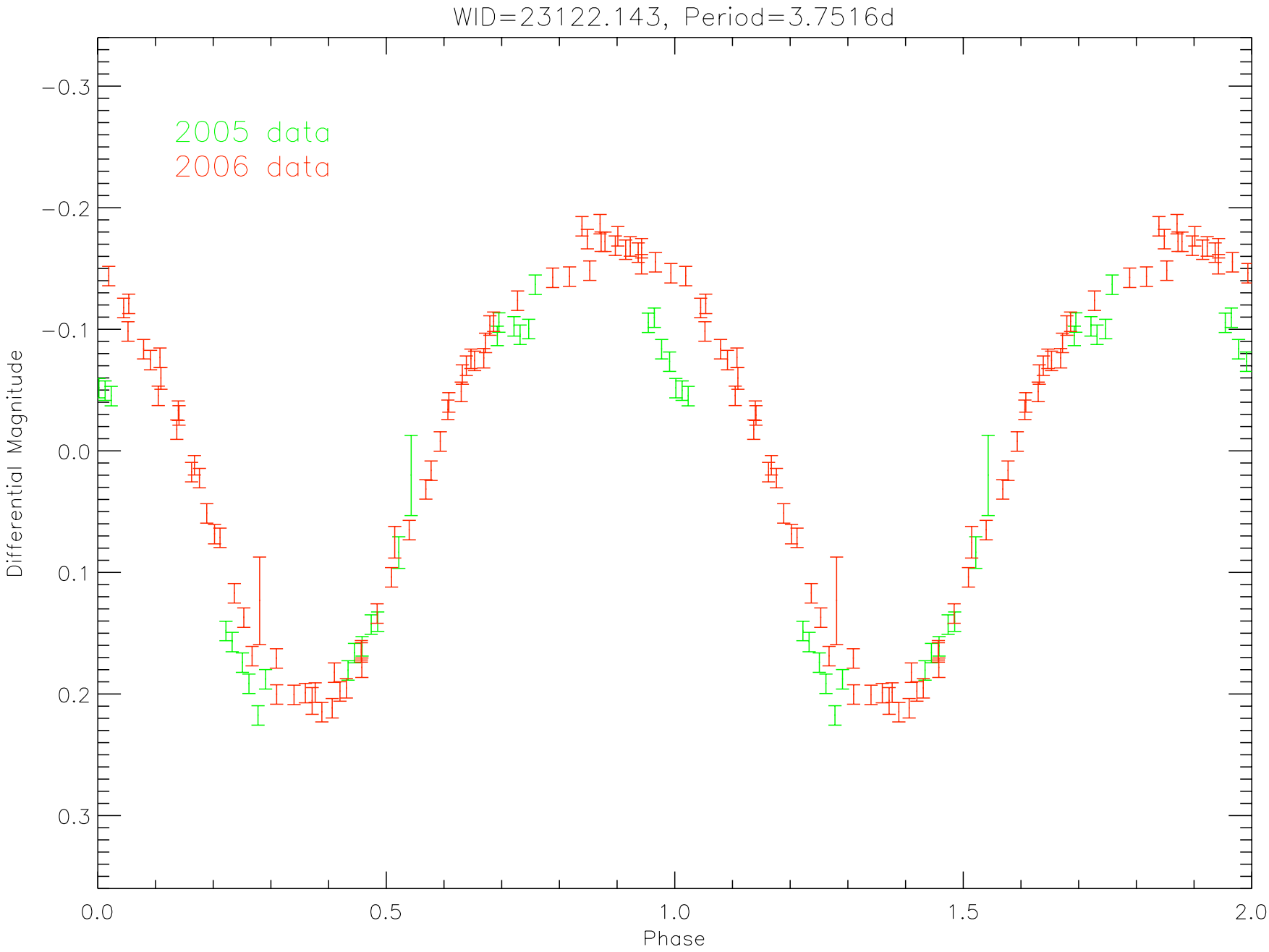
WID=23122.143, Period=3.7516d
2005 data
2006 data
Differential Magnitude
−0.3
−0.2
−0.1
0.0
0.1
0.2
0.3
0.0
0.5
1.0
1.5
2.0
Phase

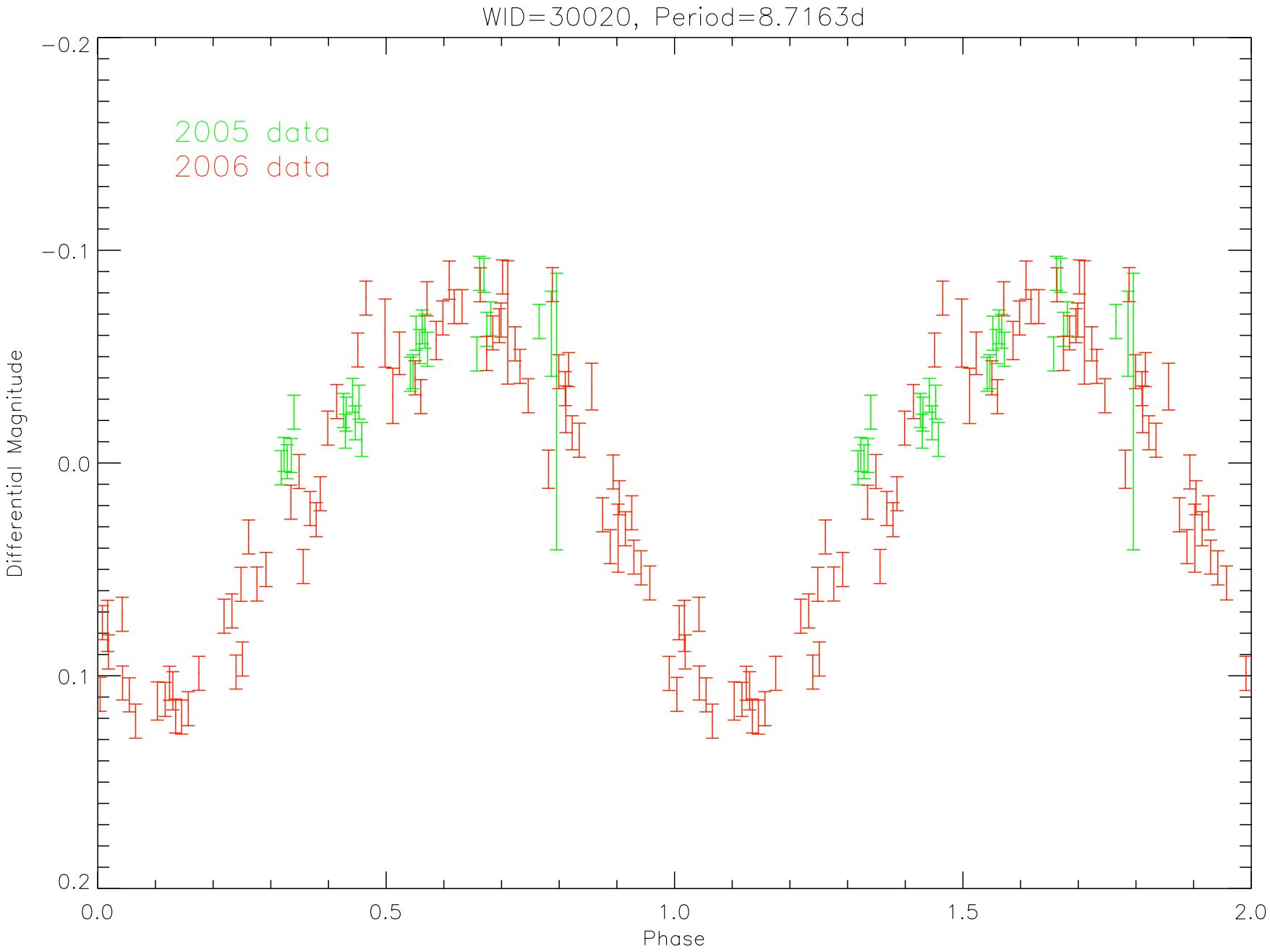
WID=30020, Period=8.7163d
2005 data
2006 data
Differential Magnitude
−0.2
−0.1
0.0
0.1
0.2
0.0
0.5
1.0
1.5
2.0
Phase

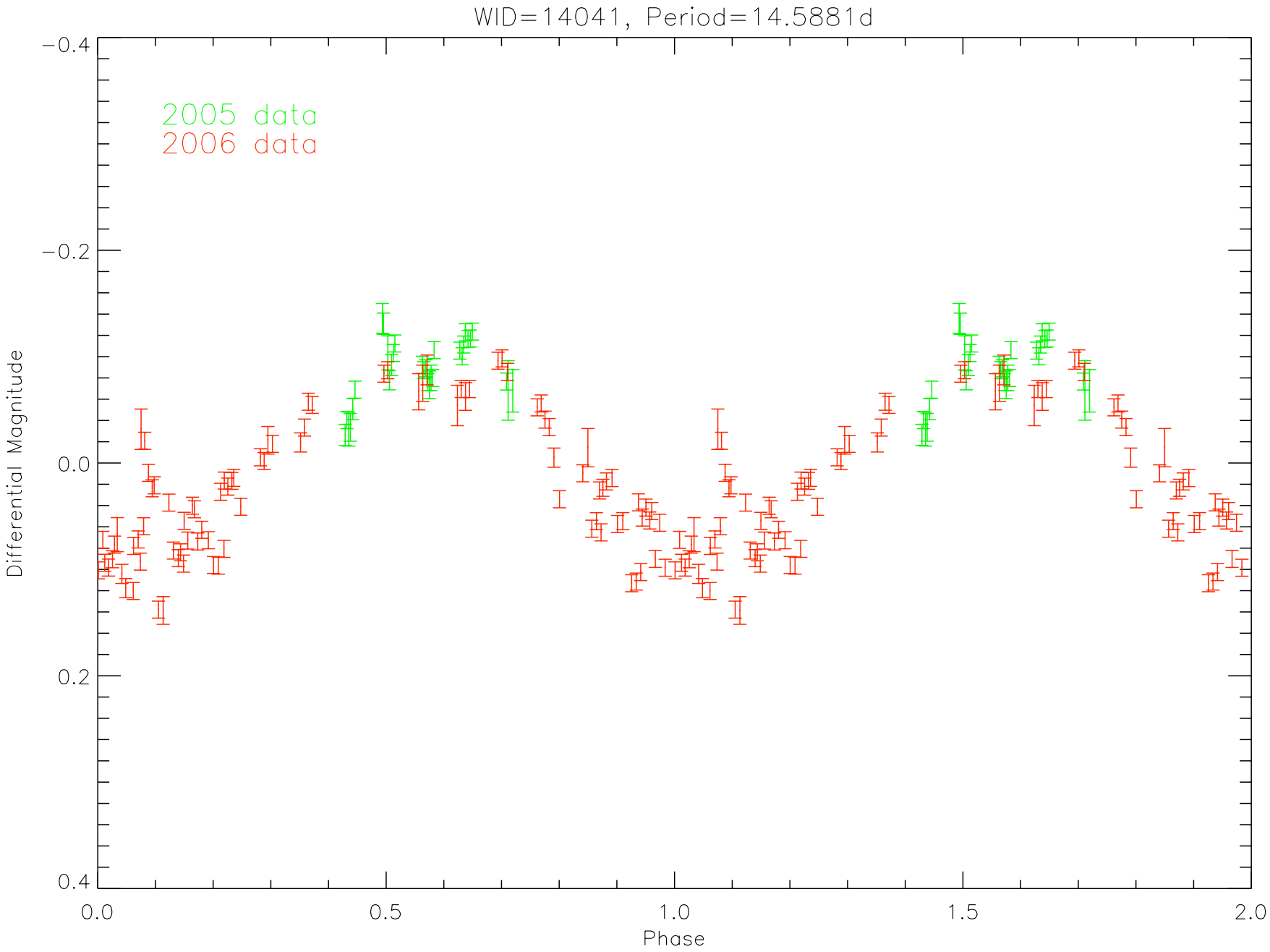
WID=14041, Period=14.5881d
2005 data
2006 data
Differential Magnitude
−0.4
−0.2
0.0
0.2
0.4
0.0
0.5
1.0
1.5
2.0
Phase